International Geology Review, Vol. 45, 2003, p. XXX–XXX.

Timing and Nature of Tertiary Plutonism and Extension in the Grouse Creek Mountains, Utah

ANNE E. EGGER,[1, 2] TREVOR A. DUMITRU, ELIZABETH L. MILLER,[1] CHARLES F. I. SAVAGE[3]

Department of Geological and Environmental Sciences, Stanford University, Stanford, CA 94305

AND JOSEPH L. WOODEN

U.S. Geological Survey, 345 Middlefield Road, Menlo Park, California 94025

Abstract

The Grouse Creek–Albion–Raft River metamorphic core complex in northwestern Utah and southern Idaho is characterized by several Tertiary plutons with a range of ages and crosscutting relations that help constrain the timing of extensional deformation. In the Grouse Creek Mountains, at least three distinct, superimposed, extension-related Tertiary deformational events are bracketed by intrusive rocks, followed by a fourth event, motion on range-bounding faults.

The Emigrant Pass plutonic complex was emplaced at depths of less than 10 km into Permian-age rocks. SHRIMP U-Pb zircon analysis indicates a three-stage intrusion of the complex at 41.3 ± 0.3 Ma, 36.1 ± 0.2 Ma, and 34.3 ± 0.3 Ma. The two youngest phases represent distinctly younger intrusive event(s) than the oldest phase, separated by more than 5 m.y. The oldest phase cuts several metamorphosed and deformed younger-on-older faults, providing a pre–41 Ma age bracket for oldest extension-related deformation in the region. The youngest phase(s) are interpreted to have been intruded during development of a map-scale, N-S–trending recumbent fold, the Bovine Mountain fold, formed during vertical shortening of roof rocks during intrusion. This second event folded older normal faults that are likely pre–41 Ma. Zircons from the youngest part of the pluton show inheritance from Archean basement (~2.5 Ga) and from its Proterozoic sedimentary cover (~1.65 Ga).

The Red Butte pluton, emplaced at 15–20 km depth, intruded highly metamorphosed Archean orthogneiss at 25.3 ± 0.5 Ma; cores of some zircons yield latest Archean ages of 2.55 Ga. The pluton is interpreted to have been intruded during a third deformational and metamorphic event that resulted in vertical flattening fabrics formed during NW to EW stretching, ultimately leading to thinning of cover and top-to-the west motion on the Ingham Pass fault. The Ingham Pass fault represents an important structure in the Grouse Creek Mountains, as it juxtaposes two parts of the crust that apparently resided as much as 10 km apart (in depth) at times as young as the Miocene.

The varied structural, metamorphic, and intrusive relations observed in the Grouse Creek Mountains reflect their formation at different levels within the crust. Data from these various levels argue that plutonism has been a key mechanism for transferring heat into the middle and upper crust, and localizing strain during regional extension. Interestingly, events documented here correlate in a broad way with cooling events documented in the Raft River Mountains, although plutons are not exposed there. Major and trace element geochemistry imply a crustal component in all of the studied plutons, indicating significant degrees of crustal melting at depth during extension, and point to mantle heat sources during the timespan of Basin and Range extension as the cause of melting.

Basin and Range faulting and final uplift of the range is recorded by apatite fission track ages, averaging 13.4 Ma, and deposition of about 2 km of syn-faulting basin fill deposits along the Grouse Creek fault mapped along the western flank of the range. Similar apatite ages from the Albion Mountains to the north indicate that the western side of the Albion–Raft River–Grouse Creek core complex behaved as a single rigid crustal block at this time.

[1]Corresponding authors; email: eggera@sanjuancollege.edu and miller@pangea.stanford.edu
[2]Department of Geology and Geography, San Juan College, 4601 College Boulevard, Farmington, New Mexico 87402.
[3]Network Solutions, 10075 Westmoor Drive, Suite 200, Westminster, Colorado 80021.

Introduction

THE ROLE THAT magmatism plays with regard to extension is one of the many controversial issues surrounding the formation and exhumation of Tertiary metamorphic core complexes in the western United States Basin and Range province. Many popular models for core complex formation, including the rooted detachment model (Wernicke, 1981) and the rolling hinge model as first described by Buck (1988) do not advocate plutonism as playing a significant role in core complex formation, yet plutons that are broadly syn-extensional are ubiquitous in many of the core complexes of the Basin and Range. Other workers argue that plutonism is the main driver for core complex formation. By supplying heat to the upper and middle crust, plutonism localizes ductile flow and extension, with a resulting component of vertical uplift due to the buoyant rise of magmas through the crust (e.g., Anderson, 1988; Lister and Baldwin, 1993; Brun et al., 1994; E. Miller et al., 1999). Detailed mapping, geochronology, and thermochronology of the generally complicated structural and metamorphic relations in the lower plates of core complexes are key to providing additional data with which to address these questions.

Most of the core complexes of the Basin and Range are situated in a narrow belt within the eastern part of the province and, as first suggested by Coney (1980), may be localized within a zone of crust previously thickened during Mesozoic thrust faulting. Referred to as "windows into the midcrust" (McCarthy and Brown, 1986), core complexes expose rocks that have been at least metamorphosed and deformed, and in many cases intruded by Tertiary plutons. Thus, although they are limited in distribution, core complexes provide the opportunity to gather key evidence for deep-seated processes during extension.

Two Tertiary plutonic complexes, yielding a range of ages, help document a history of episodic magmatism, metamorphism, and deformation in the Grouse Creek Mountains of the Albion–Raft River–Grouse Creek metamorphic core complex (Fig. 1), and make this region an ideal one in which to examine the relationship between plutonism and extension. Previous workers have investigated the structural, magmatic, and metamorphic history of several parts of the complex. These workers include Compton et al. (1977), Todd (1973, 1980) and Compton (1983) in the Grouse Creek Mountains; Armstrong and Hills (1967), D. Miller (1980), D. Miller et al. (1990), D. Miller and Bedford (1998), and Forrest et al. (1994) in the Albion Mountains; Saltzer and Hodges (1988) in the Middle Mountain area; and Compton (1972, 1975), Compton et al. (1977), Malavielle (1987a, 1987b), Wells (1997), and Wells et al. (1997a, 1998, 2000) in the Raft River Mountains. The combined field observations and geochronologic work by these authors highlight the spatial association of inferred extensional fabrics with either plutons or significant metamorphic heating and/or cooling events throughout the core complex, but in detail, the relations described between deformation, metamorphism, and plutonism vary, and have not been clearly outlined.

This study focuses on the central and southern Grouse Creek Mountains (Figs. 1 and 2), where two Tertiary plutonic complexes of different age and with dramatically different intrusive relations constrain the timing of extension in surrounding wall rocks. The southern plutonic complex is older and was intruded into high levels of the crust, whereas the northern pluton is younger and was intruded at much deeper levels of the crust. Between the two plutons, low-angle faults defined by breaks in the metamorphic grade and age of rock units have been identified; these excise or remove parts of the structural section, exposing differing crustal levels in different parts of the range (Fig. ochronana
thrm(ocn)5.5r(on)5.5ohog ,a ocem
plutoic com-5.8(plexts)-5.3elpn carify c lo(og)-5.6(icmea)-5.6p
an-5.1(dpn-5.1en)-0.3t ro65.1gnic s-174
nmp(ton et ala, 177; (T)7475oh)0d,s
0(og)-5.3(ic(relatio)-6.2(s3(s in)-6.3(the)]TJ0 -1.1899 TD0.33
vents spnnded 16.lrdpn-562(e)0.2(io(d rcom)]T.
mi439(d- crusi439(a)0(lx,)6.3provmi439(dmi439(ing(an-5.4((ex

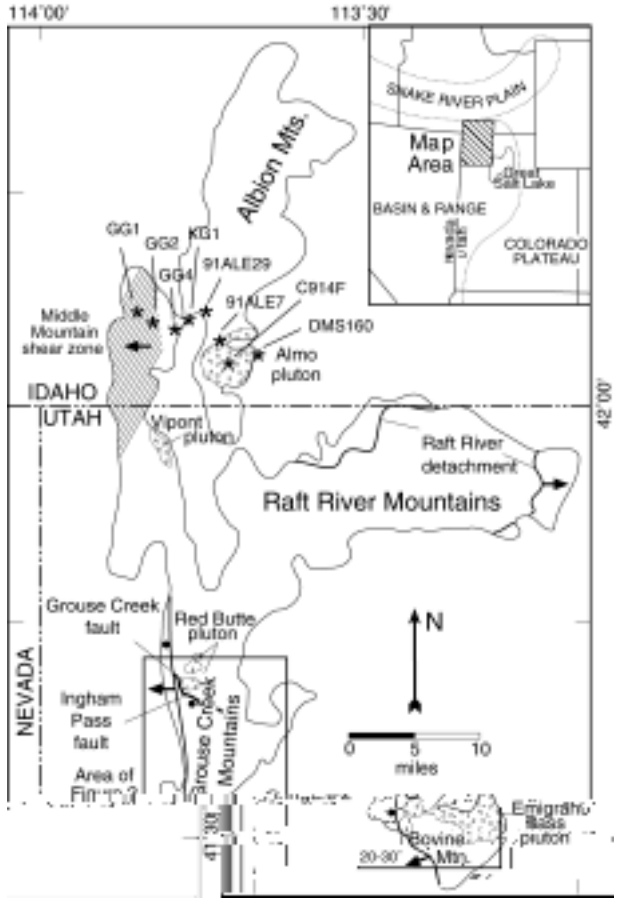

FIG. 1. Location map of study area showing places and structures discussed in text. Asterisks and numbers in the Albion Mountains show the approximate location and relative position/spacing of fission-track samples discussed in text. Latitude and longitude of each sample are listed in Table 2 and age data are compiled in Figure 13.

southern extension of this large core complex (Figs. 1 and 2).

The core of the Grouse Creek Mountains consists of 2.5 Ga orthogneiss in which older metasedimentary rocks are less abundantly exposed as screens or pendants (Compton et al., 1977; Todd, 1973, 1980). The Archean orthogneiss is unconformably overlain by a sequence of Proterozoic metasedimentary rocks (Fig. 2). The overlying Paleozoic represents part of a thick wedge of passive margin carbonate and siliciclastic rocks similar to that present throughout western North America (Compton et al., 1977; Wells et al., 1998). These units are thinned and/or faulted throughout the range, a result mainly, but possibly not entirely, of Tertiary-age deformation (for differing views, see Compton et al., 1977; Wells et al., 1997a). Despite extensive Tertiary deformation and metamorphism, parts of the Grouse Creek–Albion–Raft River complex preserve evidence for older Mesozoic metamorphism and deformation. Published data point to a Late Cretaceous age, or Late Cretaceous cooling age, for this metamorphism.

In support of a Cretaceous age, eight conventional K-Ar ages on biotite, muscovite, and hornblende, ranging from 66 to 81 Ma were obtained by Armstrong (1970) and Armstrong and Hills (1967) in parts of the Albion Range where rocks exhibit the oldest documented deformational/metamorphic fabrics (D. Miller, 1980). Forrest et al. (1994) reported $^{40}Ar/^{39}Ar$ muscovite ages increasing from 65 to 82 Ma with greater distance from the Cenozoic Almo pluton in the Albion Mountains, where fabrics bear

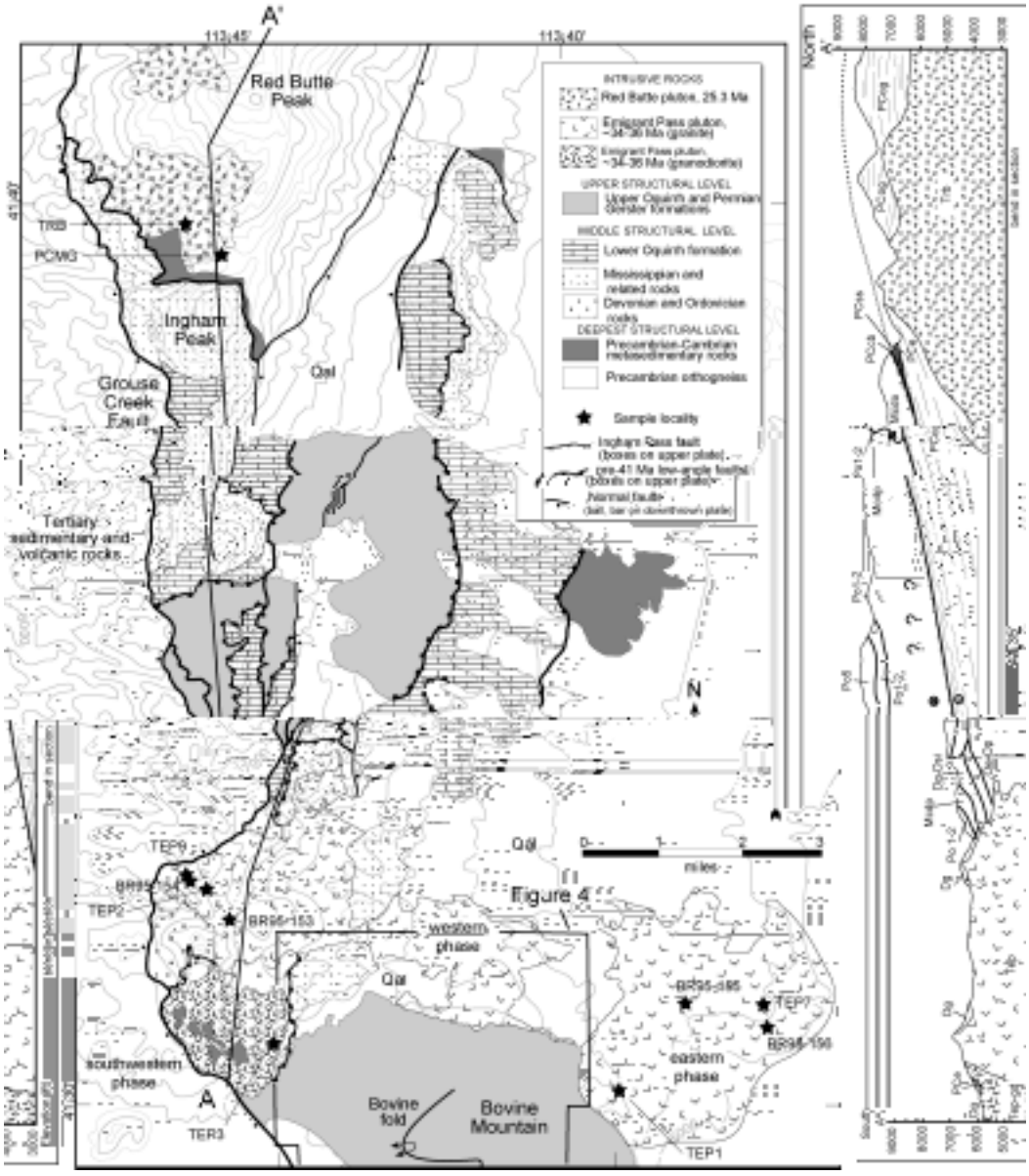

FIG. 2. Simplified geologic map of the Grouse Creek Mountains, showing places, features, and sample localities discussed in text. Sources of data for geologic mapping and cross-section include Compton (1983), Todd (1980), the Stanford Geological Survey (unpubl. data, 1988), and Egger (2001). Latitude and longitude of fission-track samples are listed in Table 2 and compiled together with Albion Mountain data in Figure 13.

evidence of both older (pre-Tertiary) and younger (Tertiary) deformational events, suggesting an 82 Ma minimum age for older Mesozoic deformation and metamorphism. Wells et al. (1990) reported three muscovite Ar/Ar plateau ages between 88 and 90 Ma from Ordovician rocks that display the oldest observed deformational fabrics in the eastern Raft River Mountains. Laser fusion ages of phlogopite in D1 strain fringes in the Oquirrh Group of the northern Grouse Creek Mountains yield ages that range

from 92 to 109 Ma, with a mean age of 102 Ma, and are interpreted as mineral growth ages that directly date an older pre-Tertiary metamorphic event (Wells et al., 2000). Higher-grade, staurolite ± garnet, ± kyanite ± sillimanite ± andalusite-bearing metamorphic rocks occur sporadically through the Albion–Raft River–Grouse Creek metamorphic complex (Compton et al., 1977) but have never been directly dated. Data from this paper provide support for conclusions of Todd (1973, 1980) and Compton et al. (1977) that at least some of the higher-grade metamorphic mineral assemblages are clearly Cenozoic in age.

In the southern Grouse Creek Mountains, the 41–34 Ma Emigrant Pass plutonic complex (this paper) cuts a series of faults that omit structural and stratigraphic section (Fig. 2; Egger, 2001). The plutonic complex contains blocks or pendants of foliated, deformed Devonian Guilmette Formation juxtaposed against pendants of Proterozoic Elba Quartzite, providing evidence for a pre-intrusive fault with significant stratigraphic offset. The plutonic rocks are not deformed. South of the Emigrant Pass pluton lies Bovine Mountain, where the map-scale recumbent Bovine fold overturns a large section of only slightly metamorphosed Ordovician–Permian strata (Jordan, 1983; this paper).

The 25 Ma Red Butte pluton intrudes the central part of the Grouse Creek Mountains (Compton et al., 1977; Todd, 1980; this paper) and is inferred to be syn-tectonic with respect to WNW- to E-W–trending stretching lineations that increase in intensity of development beneath the Ingham Pass fault. The Ingham Pass fault is the most significant structural and metamorphic break in the Grouse Creek Mountains, inasmuch as it separates greenschist-facies Paleozoic rocks in the upper plate from more highly metamorphosed and deformed lower-plate rocks of dominantly Proterozoic and Archean age that, based on metamorphic assemblages, resided at ~15–20 km depths in the Miocene (Fig. 2).

The Grouse Creek Mountains are bounded on the west by the Grouse Creek fault, which places a thick Miocene sedimentary sequence against Paleozoic and Precambrian rocks (Fig. 2). Southwest of the range, 11–14 Ma rhyolite plugs intrude Tertiary sediments, placing an upper age bracket on the succession (Compton, 1983). Lesser offset, high-angle normal faults bound the eastern side of the range (Fig. 2).

Geologic mapping at 1:24,000 or greater scale has been carried out by Stanford University faculty and students in the Grouse Creek Mountains over ~30 years. Todd (1973) completed a Ph.D. thesis in the central Grouse Creek Mountains. The Stanford Geological Survey (summer field camp program) mapped the Grouse Creek region during 1973 and 1976 under the direction of Bob Compton, and during 1988 under the direction of Elizabeth Miller. Egger (2001) completed an M.S. thesis in the southern and central Grouse Creek Mountains, and a Ph.D. thesis in progress by Martinez describes the Tertiary succession on the west side of the Grouse Creek Mountains. Geologic mapping in the Grouse Creek Mountains has been published by Todd (1973, 1980), Compton (1983), and Jordan (1983), and compiled 7.5' quadrangle mapping has been submitted to the Utah State Geologic Survey by Egger for the Emigrant Pass and Potter's Creek quadrangles. Compilation of geologic maps of the Bovine and Rocky Pass Peak 7.5' quadrangles are currently in progress (Martinez, in progress; Martinez and Egger, in progress). All supporting 1:24,000 geologic mapping and structural cross-sections that form the basis for the discussion of geochronologic data presented here are included in Egger (2001).

Tertiary Plutons

Emigrant Pass plutonic complex

The Emigrant Pass plutonic complex is a large, three-part granitoid body intruded into Precambrian through Permian rocks at the southern end of the Grouse Creek Mountains (Fig. 2). The petrography of the pluton has been described in detail by Baker (1959). The plutonic complex is elongate in an E-W direction, and is situated along the boundary between structurally thinned and metamorphosed Paleozoic rocks of the central Grouse Creek Mountains to the north and the feebly metamorphosed rocks of Bovine Mountain to the south (Fig. 2). The pluton is also characterized by a steep gravity gradient parallel to the long axis of the pluton (Cook et al., 1964). This steep gradient, lower to the south, likely represents a pre-existing structural weakness, possibly a down-to-the-south Mesozoic or early Cenozoic normal fault that may have facilitated intrusion of the Emigrant Pass plutonic complex to fairly shallow levels of the crust over a 7 m.y. time span (discussed below).

A narrow (~20 m) but well-developed contact aureole around the Emigrant Pass plutonic complex contains mineral assemblages that include wollastonite, sillimanite, and andalusite (Fig. 3). Andalusite

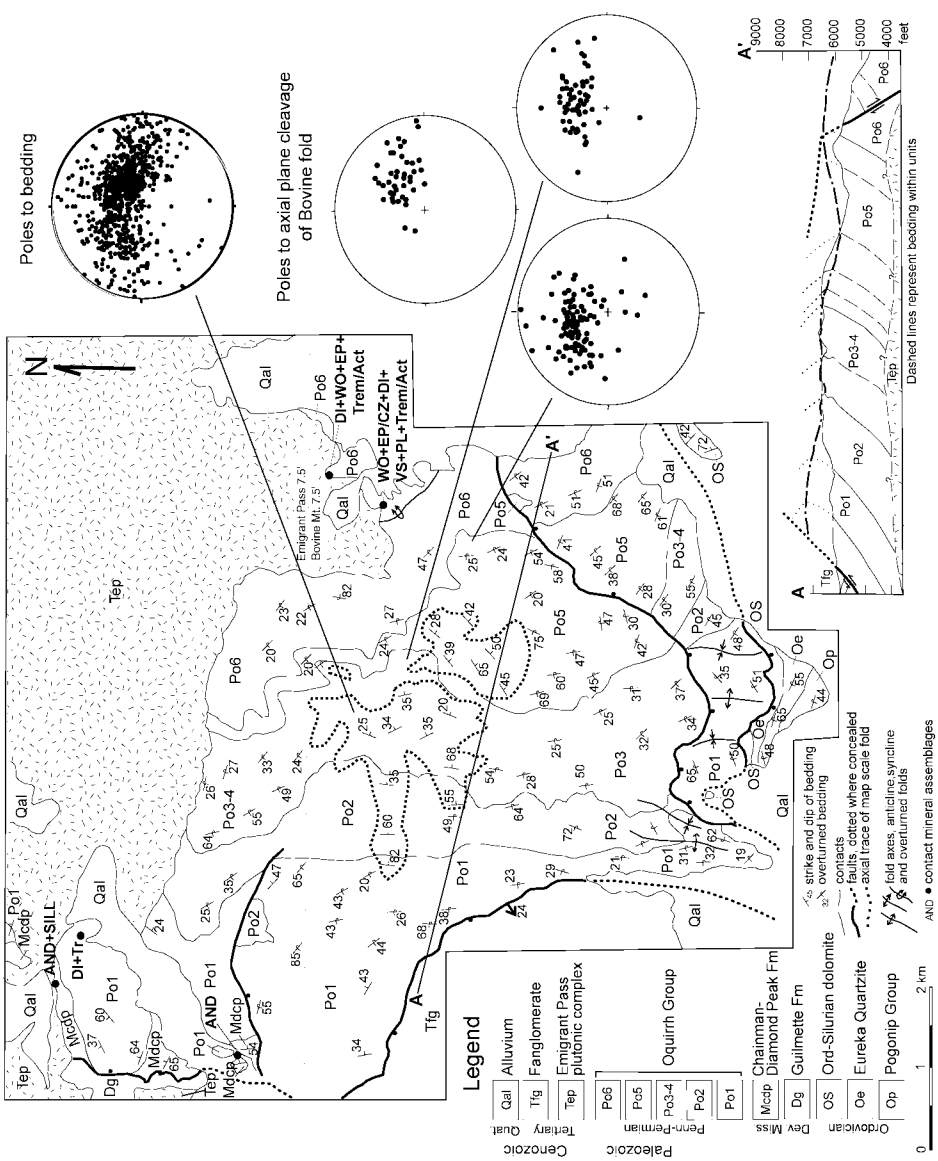

FIG. 3. Simplified geologic map and cross-section of Bovine Mountain showing compiled structural data defining the Bovine fold. Based on geologic mapping and data collection by the Stanford Geological Survey (unpubl. data, 1988).

+ sillimanite in contact-metamorphosed exposures of the Mississippian Chainman Shale (Fig. 3) indicate elevated temperatures at pressures beneath the aluminum-silicate triple junction (less than 12 km depth). Wollastonite, formed by the reaction quartz + calcite, indicates elevated temperatures (likely above 500°C) at pressures lower than the aluminum-silicate triple junction (Greenwood, 1967; Spear and Cheney, 1989) . The Pennsylvanian–Permian Oquirrh Group sediments at Bovine Mountain, away from pluton contacts, contain widespread tremolite-actinolite-epidote-chlorite of inferred Tertiary age (discussion below) implying greenschist facies conditions and temperatures no higher than 200-400° C (Egger, 2001). Stratigraphic thickness of the Pennsylvanian–Permian and overlying Triassic section across this region is about 5 km. Together, these data indicate depths of intrusion probably no more than 5–10 km for the Emigrant Pass plutonic complex. The Emigrant Pass plutonic complex cuts a series of section-omitting normal faults, which also represent metamorphic breaks. Near the northernmost extent of the outcrop of plutonic rocks, the lower Oquirrh Group is more coarsely recrystallized and contains metamorphic muscovite. It is structurally overlain by less metamorphosed siltstones and silty limestone of the upper Oquirrh Group in the hanging wall (Figs. 2 and 3; Egger, 2001). This older metamorphism remains undated. The lack of recrystallization and metamorphic mineral growth in the upper Oquirrh suggests that these units were juxtaposed by motion along a fault that post-dated greenschist-grade metamorphism and pre-dated intrusion of the cross-cutting Emigrant Pass pluton (Fig. 2; Egger, 2001). Samples from near the contact of the plutonic complex yield muscovite ages of about 34 Ma, compatible with cooling of country rocks shortly after intrusion (Egger, 2001).

South of and above (?) the plutonic complex, a map-scale, recumbent fold beneath Bovine Mountain overturns a thick (4 km+) section of Pennsylvanian–Permian limestone, sandy limestone, sandstone, and siltstone of the Oquirrh Group and appears to fold faults that are at high angles to bedding and omit section at the southern end of the range (Figs. 2 and 3; see also Jordan, 1983). Jordan (1983) divided the Oquirrh Group into six informal units in the Bovine Mountains. Subunits 3 and 4 are difficult to distinguish and are grouped together on the simplified map depicted in Fig. 3. These units are mostly overturned beneath Bovine Mountain and are upright only above the axial trace of the fold. The main foliation or cleavage associated with this folding is a penetrative (in shalier units) to spaced cleavage (in sandier units) that is axial planar to the map-scale Bovine fold (Figs. 4A and 4B). This cleavage increases in intensity and becomes more penetrative structurally downward toward the roof of the pluton; likewise, metamorphic grade increases with increasing strain structurally downward. Chlorite and fine-grained white mica, for instance, define the axial planar cleavage at the highest structural levels; at deeper levels near the pluton contacts, coarser muscovite and chlorite define this same cleavage. Smaller scale folds, where present, are tight to isoclinal where strain is high near the pluton, and moderate to tight at higher structural levels. Along the contact with the pluton, the axial planar fabric is overprinted in a static fashion by contact metamorphic minerals. Locally, thin aplite dikes are involved in the deformation (Figs. 4C and 4D), whereas most others are clearly crosscutting.

Based on field observations, structural data, and geologic mapping (Fig. 3), we interpret the formation of the fold on Bovine Mountain as synchronous with the intrusion of at least the two younger phases of the Emigrant Pass plutonic complex (Fig. 2). This interpretation differs from that of Jordan (1983) in that she interpreted the formation of the fold as pre-intrusive. Jordan described three sets of folds, and she included the map-scale Bovine fold in the second fold category. Based on data discussed above, it appears that the main folding event was associated with cleavage development, and because only one main foliation or cleavage characterizes the Oquirrh Group rocks of Bovine Mountain (Fig. 3) this cleavage is believed to be associated with a *first* folding event, not a second, as it cuts and folds bedding, but not an earlier foliation (Figs. 3 and 4). Evidence that this fold developed during intrusion of the Emigrant Pass plutonic complex includes the fact that the observed axial planar cleavage of the Bovine fold increases in intensity of development and becomes more penetrative structurally downward towards the mapped edge and inferred roof of the pluton. Similarly, metamorphic grade increases with increasing strain structurally downward to the roof of the pluton. The axial plane of the fold and axial planar cleavage dip at a low angle, and are subparallel to the inferred top of the plutonic complex (Fig. 3).

The simplest explanation for the origin of the Bovine fold is that the stratigraphic section was already faulted and tilted prior to intrusion of the

FIG. 4. Photographs of key relationships at Bovine Mountain. Figures 4A and 4B show gently dipping cleavage at an angle to bedding. This cleavage is axial planar to the map-scale Bovine fold. Note better development of cleavage in finer-grained silty beds and its absence in coarser-grained sandstone and conglomerate (Fig. 4B). Figures 4C and 4D are photographs of aplite dikes emanating from the eastern phase of the Emigrant Pass plutonic complex that are variably deformed (stretched and boudinaged [Fig. 4C] or folded [Fig. 4D] by cleavage that is axial planar to the Bovine fold).

Emigrant Pass plutonic complex; heating allowed tilted strata to undergo sub-vertical flattening, forming the recumbent fold and its gently dipping axial planar cleavage. The fold axis of the Bovine fold, based on plots of poles to folded bedding and plots to poles to axial plane cleavage (which fan somewhat about the fold axis due to cleavage changing angles in different lithologies), is approximately N-S, parallel to structures considered by workers in the region to be related to Mesozoic deformation. The N-S orientation of this map-scale recumbent fold is compatible, however, with our conclusion that it is Cenozoic in age, provided that units dipped east or west with an approximate N strike prior to folding about a subhorizontal axial plane. These relationships provide additional evidence that the stratigraphic section was already faulted and tilted prior to intrusion.

Geochronology. The Emigrant Pass plutonic complex was previously dated at 38.2 ± 2.0 Ma based on a six-point Rb-Sr whole-rock isochron (Compton et al., 1977). These authors noted, however, that the pluton consists of three lobes or phases (Fig. 2), and suggested that the 38 Ma age may have been strongly influenced by data from the southwestern part of the pluton. Armstrong (1970) reported a biotite K-Ar age of 23.3 Ma for the northwestern part of the pluton. D. Miller et al. (1990) reported a hornblende K-Ar age of 49.2 ± 1.2 Ma from a gabbro boulder in the Tertiary section west of the Grouse Creek fault, which compositionally and texturally resemble mafic dikes within the pluton. The age discrepancies have been variously interpreted as due to multiple intrusions, slow cooling and/or continuous heating, argon loss (in biotite) and/or excess argon (in hornblende), or resetting of biotite ages due to a later heating event, possibly associated with intrusion of the Red Butte pluton.

To resolve this issue, samples from all three phases of the plutonic complex were analyzed on the SHRIMP-RG facility at Stanford University.[4] The three phases of the Emigrant Pass plutonic complex

[4]See Figure 2 for sample locations and Figure 5 for cathodoluminescence (CL) images of zircons dated. SHRIMP analytical data for all samples are included in the Appendix Tables A1–A7).

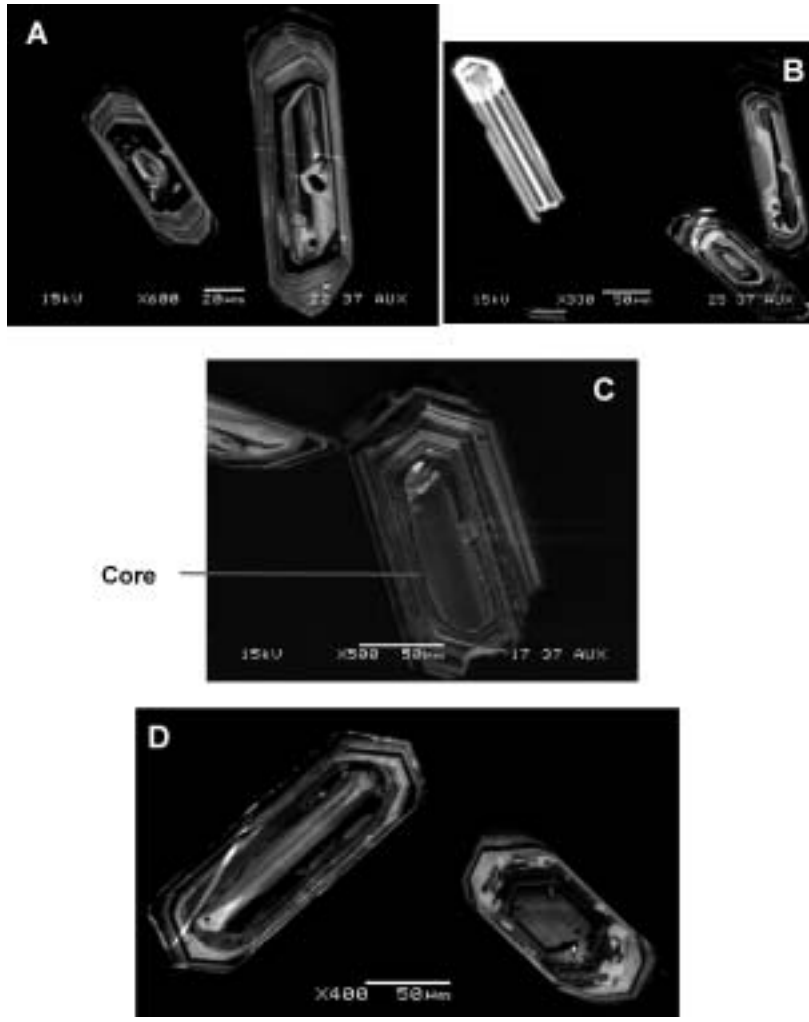

FIG. 5. Cathodoluminescent images of representative zircons from samples analyzed with SHRIMP. A. Zircons from sample TEP3. B. Zircons from sample TEP2. The regular zoning is typical of zircons from the entire sample. C. Zircons from TEP1. Note anhedral core and regularly zoned rim. The cores of these zircons yield Proterozoic U-Pb ages, whereas rims yield Tertiary ages. D. Zircons from sample TRB. Grain on left has a latest Archean core with a Tertiary rim; grain on right is 25 Ma magmatic zircon.

differ at both the hand-sample and thin-section scale, but clear crosscutting relationships are buried under Quaternary cover or otherwise obscured (Fig. 2), except for the presence of cross-cutting aplite dikes in the more mafic western phase of the plutonic complex, described below. The chronological separation of three intrusive phases of the plutonic complex rests mainly upon the geochronology of zircons from the three phases. The southwestern phase intruded at 41.3 ± 0.3 Ma (Fig. 6), the northwestern phase at 36.1 ± 0.2 Ma (Fig. 7), and the most voluminous eastern phase at 34.3 ± 0.3 Ma (Fig. 8A). All errors reported are 1σ.

The southwestern phase of the Emigrant Pass plutonic complex (Tepgd and Sample TEP3) is the smallest and most heterogeneous portion of the complex. Composition and texture vary from fine-grained diorite to coarse-grained granodiorite. Abundant mafic xenoliths 1–10 cm in length occur in small zones along the southern margin, as do

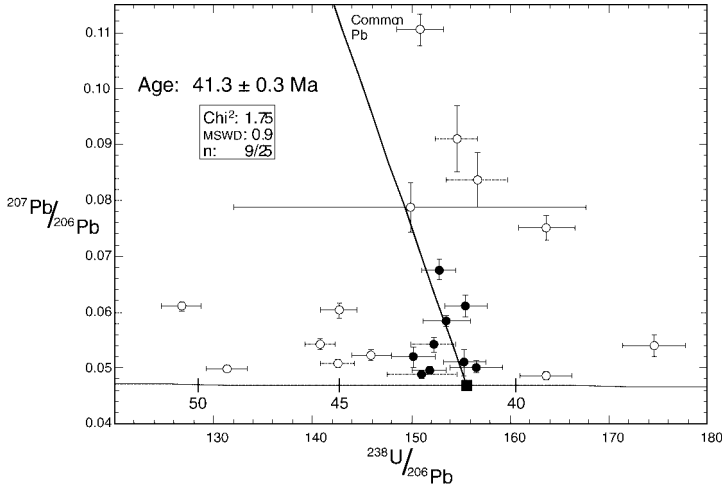

FIG. 6. Tera-Wasserburg plot of SHRIMP data from TEP3. Solid circles represent data used to determine age.

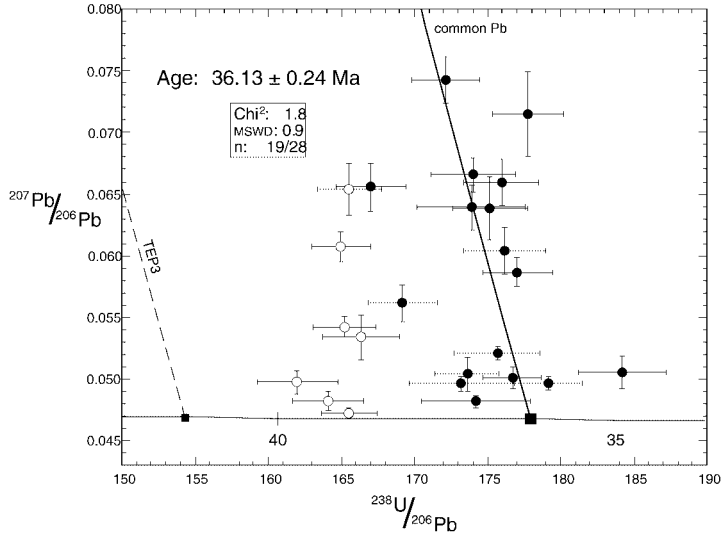

FIG. 7. Tera-Wasserburg plot of SHRIMP data from TEP2. Solid circles represent data used to determine reported age.

dikes and enclaves with phenocrystic hornblende up to 2 cm in length. Less abundant aplite dikes cut these lithologies and are likely related to the intrusion of the later phases. The southwestern phase also contains numerous large blocks of Precambrian Elba Quartzite and Devonian Guilmette Formation (Fig. 2). The juxtaposition of blocks of two widely separated stratigraphic units can possibly be explained by the presence of a major, pre-intrusive, down-to-the-south fault, as also suggested by gravity data (Cook et al., 1964).

Sample TEP3 (Fig. 2) is a medium-grained, hypidiomorphic granodiorite typical of the bulk of the southwestern phase of the plutonic complex. Zircons from TEP3 are clear, euhedral, and needle-like, with regular zoning under cathodoluminescence (CL) (Fig. 5). Twenty-five analyses representing data uncorrected for common Pb are plotted in Figure 6.

Although none of the grains are concordant, 9 out of 25 analyses define a weighted mean age of 41.3 ± 0.3 Ma. Many grains show signs of Pb loss, plotting to the right of the common-Pb line—this is likely a result of continued heating during intrusion of later phases of the plutonic complex. Several grains plot to the left of the common-Pb line, indicating an inherited component, though no older cores were found in these grains. Given the compositional and textural variability of this phase, however, it is reasonable to conclude that these grains could be inherited from yet an earlier phase of the same pluton.

The northwestern phase of the Emigrant Pass plutonic complex (TEP2) crosscuts a low-angle fault between strongly foliated Devonian Guilmette Formation and lower-grade Mississippian Chainman–Diamond Peak Formation (Figs. 2 and 3). Garnetiferous aplite dikes cut the surrounding country rocks.

Sample TEP2 is coarse-grained biotite granite typical of the northwestern phase of the complex. CL shows clear, needle-like zircons with regular zoning, similar to sample TEP3 (Fig. 5). Twenty-eight analyses representing data uncorrected for common Pb are presented in Figure 7. Although the data are widely scattered, data from TEP2 demonstrate the tightest clustering of the three plutonic phases, and 19 of the 28 analyses were used to determine a weighted mean age of 36.1 ± 0.2 Ma. As with TEP3, some grains show Pb loss due to subsequent reheating, probably during younger magmatism, and those grains that appear to plot along concordia to older ages likely indicate inheritance from the earlier southwestern lobe. No older cores were detected in any of the zircons of TEP2 (Fig. 5).

The eastern phase of the Emigrant Pass plutonic complex (TEP1) is the most extensive in outcrop area (Fig. 2). The southern margin of this pluton consists almost entirely of aplite and pegmatite dikes; the rest of the pluton is a virtually homogeneous coarse-grained biotite granite.

Sample TEP1 is a coarse-grained, hypidiomorphic granite (Fig. 2). CL of zircons reveals anhedral cores surrounded by euhedral rims with regular zoning (Fig. 5). Some cores show regular zoning, while others are metamict and retain little of their original crystal structure.

Twenty-four analyses representing data uncorrected for common Pb are shown in Figure 8A, with a weighted mean age of 34.3 ± 0.2 Ma based on 12 data points. Again, some Pb-loss is apparent, as well as inheritance from earlier intrusive phases. In addition, older cores in zircons from TEP1 reveal two suites of inheritance: one from a latest Archean source ~2.5 Ga and another from a Proterozoic source ~1.65 Ga (Figs. 8B and 8C). These cores probably were derived from Archean basement and the overlying Proterozoic metasedimentary rocks. Although data from the two youngest phases of the Emigrant Pass plutonic complex show some overlap, the presence of cores in TEP1 (and the lack thereof in TEP2) suggests that their statistical separation may be valid.

Compton (1983) reported a K-Ar biotite age of ~34 Ma for a crystal-rich tuff near the base of the Tertiary sedimentary section along the western side of the Grouse Creek Mountains; K-Ar analysis of sanidine from a tuff slightly higher in the section produced an average age of 33.4 ± 1.0 Ma . These ages are close to the age of intrusion of the eastern part of the plutonic complex and may represent volcanic equivalents. However, further analysis is necessary in order to link them firmly to the plutonic rocks.

Emigrant Pass pluton—summary. The above data help constrain the age of some of the structural relationships seen in the southern Grouse Creek Mountains and Bovine Mountain. Although data from the three samples dated do overlap, a histogram of $^{206}Pb/^{238}U$ ages shows three distinct peaks and justifies the assignment of different ages to the samples (Fig. 9). This unusually long period of spatially coincident intrusions may have been facilitated by a through-going crustal-scale fault, which existed prior to intrusion. The existence of this fault is based on the evidence for pre-intrusive (41 Ma) juxtaposition of strata from high in the section against the much deeper Elba Quartzite, and is interpreted as a down-to-the-east or southeast fault (Fig. 2). The contact of the western phase of the Emigrant Pass plutonic complex cuts sharply across several faults; thus motion along these faults occurred prior to 36 Ma and most likely also prior to 41 Ma. Based on the data and reasoning presented in this paper, we interpret the formation of the Bovine fold and its axial planar cleavage, which developed under greenschist-facies conditions, as syn-tectonic with the intrusion of the western and/or the eastern phases of the plutonic complex, thus constraining the formation of the fold as 36–34 Ma. There is no indication that the pluton was subsequently metamorphosed or deformed, constraining many of the section-omitting faults in this region

and much of the greenschist-facies metamorphism of the country rocks as pre–Early Oligocene, and possibly pre–Late Eocene. Clearly, the Emigrant Pass plutonic complex as a whole post-dated an important period of extensional faulting in this area. Based on data presented here, the recumbent, N-S–trending Bovine fold is Tertiary (Oligocene). In our interpretation, normal faulting that occurred prior to the final intrusion of the Emigrant Pass plutonic complex resulted in panels of tilted stratigraphic sections that were then vertically shortened/horizontally flattened, producing the cleavage and fold geometry (including folded faults) seen today on Bovine Mountain (Fig. 3).

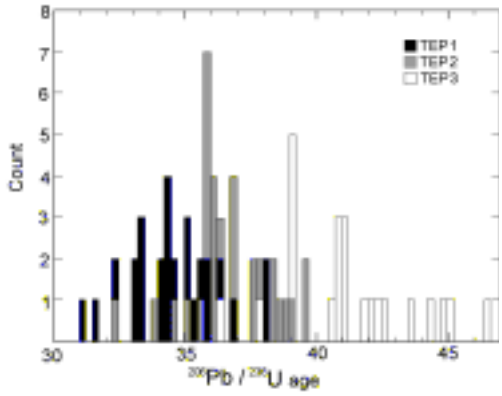

FIG. 9. A histogram of all $^{206}Pb/^{238}U$ ages obtained from zircons in all three TEP samples. The distribution of ages supports the conclusion that the three samples represent three phases of intrusion over an 8 m.y. period.

Red Butte pluton

General. The Red Butte pluton crops out exclusively in the lower plate of the Ingham Pass fault in the central part of the Grouse Creek Mountains (Fig. 2). Detailed petrologic descriptions of the rocks and intrusive relations were given by Todd (1973, 1980). The pluton intrudes Archean orthogneiss and the overlying sequence of Proterozoic metasedimentary rocks. Rocks here experienced amphibolite-facies metamorphism in the Tertiary, and metasedimentary screens within the Archean orthogneiss of pelitic composition are characterized by metamorphic assemblages that include garnet, kyanite, staurolite, sillimanite, and andalusite (Todd, 1973; Table 1 in Compton et al., 1977). Gravity data (Cook et al., 1964) and petrography suggest that only the upper zone of the Red Butte pluton is currently exposed, and that the pluton may underlie a large portion of the range, helping to explain the elevated metamorphic grade of the surrounding rocks (Todd, 1973, 1980).

The Ingham Pass fault represents a significant metamorphic and structural break. It is a low-angle fault, subsequently cut and offset by the younger Grouse Creek range-bounding fault (Figs. 1 and 2). Presently, this fault is gently dipping and has a slightly domed geometry, with a well-defined top-to-the-west sense of shear based on outcrop and thin-section data collected by the Stanford Geological Survey in 1988 and by Egger (2001). Previously, Compton et al. (1977) and Todd (1980) interpreted this fault as having moved in a top-to-the-east rather than a top-to-the west direction. Above the fault lie exposures of Mississippian Chainman Shale and younger Paleozoic units (Fig. 2) that experienced greenschist-facies metamorphism (Todd, 1973).

Below the Ingham Pass fault, lower-plate rocks host a consistent, high-strain, subhorizontal gneissic foliation (Todd, 1973, 1980). Associated with this foliation is a pervasive, high-strain, approximately N-S–stretching lineation of unknown age that formed at greenschist or amphibolite grade (Todd, 1973, 1980; Compton et al., 1977). This is overprinted by an approximately E-W lineation that increases in intensity of development toward the Ingham Pass fault. Within 500 m of the fault, the older N-S lineation is completely obliterated by the younger E-W lineation, which formed at amphibolite-facies conditions (Todd, 1973, 1980; Stanford Geological Survey, 1988, unpubl. data). The Red Butte pluton itself is mostly massive and undeformed. However, it locally exhibits a subhorizontal foliation and E-W lineation, especially near its contacts with country rock orthogneiss (Todd, 1973). It is also strongly mylonitized in a tens of meters thick zone along its western border beneath the Ingham Pass fault (Stanford Geological Survey, unpubl. data, 1988) (Fig. 2). Metamorphic and field relations indicate that the Red Butte pluton was the main source of heat during development of the second fabric and associated metamorphism (Todd, 1973).

Away from the high-strain region beneath the Ingham Pass fault, metamorphic textures are coarse and crystallization kept pace with deformation. The biotite + muscovite ± staurolite ± kyanite ± garnet ± sillimanite ± andalusite assemblage described by Todd (1973) and noted by Compton et al. (1977) indicates temperatures above 500°C and minimum intrusive depths greater than the aluminum silicate triple junction, probably at ~ 5 kbar, or at depths

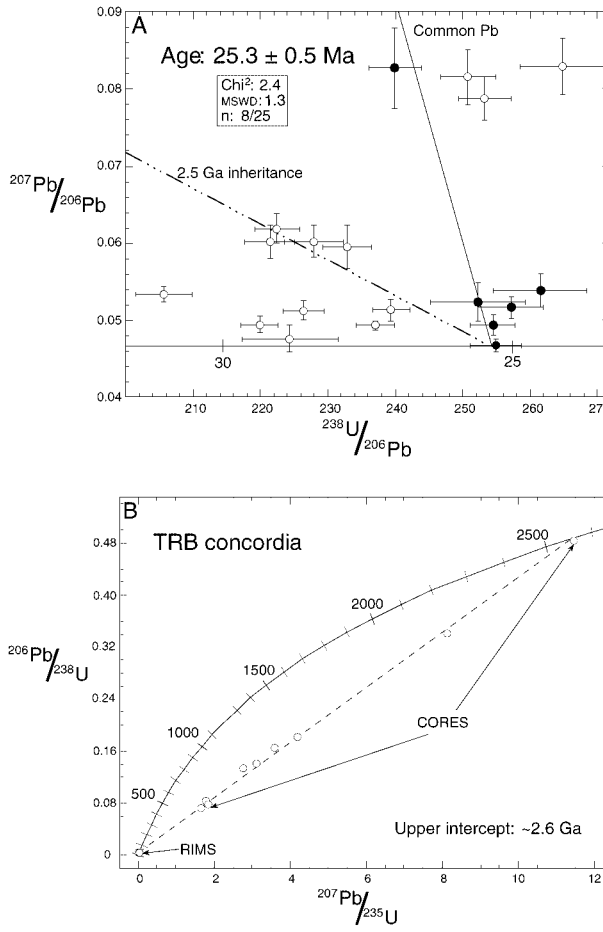

FIG. 10. A. Tera-Wasserburg plot of TRB SHRIMP data, rims only. Solid circles represent data used to define age. B. Wetherill concordia plot of TRB rim and core data.

greater than 15 km (Spear and Cheney, 1989). Todd (1980) noted that the pluton lies within the zone of maximum attenuation of the Archean orthogneiss and suggests that the orthogneiss rose diapirically, entrained with the rising pluton. All of these relationships suggest that the Red Butte pluton intruded synextensionally, underscoring the importance of accurately dating its emplacement age. The fact that the pluton is largely undeformed suggests that it mostly crystallized after deformation ceased, but that it locally acquired a solid-state fabric as rocks rose through the ductile into the brittle part of the crust (Todd, 1973). Lower-plate rocks are increasingly deformed toward the Ingham Pass fault, which is parallel to fabrics in the lower plate. The Ingham Pass fault strikes about N50–60°W and dips 20–30° SW. Final motion on the Ingham Pass fault occurred under brittle conditions. Slickensides and lineations in fault gouge measured at Ingham Pass indicate N74°W directed slip (Stanford Geological Survey, unpubl. data, 1988; Egger, 2001, 2003a, 2003b).

Geochronology. The Red Butte pluton was previously dated at 24.9 ± 0.6 Ma based on a six-point whole- rock Rb-Sr isochron (Compton et al., 1977). The sample TRB represents the main phase of the pluton: a homogeneous, coarse-grained, hypidiomorphic biotite granite. SHRIMP U-Pb zircon data confirm the age obtained by Compton et al. (1977) and indicate an age of 25.3 ± 0.5 Ma (Fig. 10A). Although the data are widely scattered, the presence of one concordant grain provides a strong anchor to the 25.3 Ma age. A few grains show Pb loss, falling

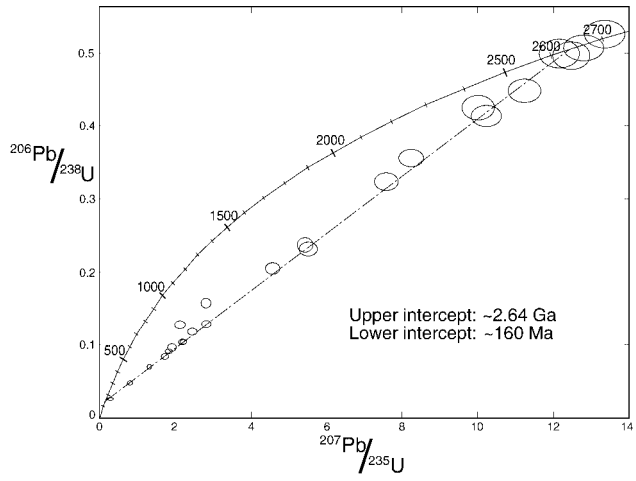

FIG. 11. Wetherill concordia plot of PCMG SHRIMP data.

to the right of the common-Pb line; this could be due to continued heating as the pluton crystallized and rose in the crust, an interpretation supported by the metamorphic relationships noted above. Data from grains trend in a direction toward inheritance and along the common-Pb line. Given the abundance of older cores (see below), this is to be expected.

Similar to the youngest lobe of the Emigrant Pass pluton, zircons from sample TRB contain inherited Archean cores whose ages define a discordia with an intercept at ~2.56 Ga, anchored by a concordant core (Fig. 10B). In samples where cores are present, CL shows well-zoned, anhedral cores surrounded by euhedral, regularly zoned rims; where no cores are present, regular zoning continues throughout the zircon grains (Fig. 5). Unlike sample TEP1, none of the cores are Proterozoic. This is expected, since intrusion of the Red Butte pluton is largely within the Archean basement (Fig. 2).

Archean orthogneiss

The orthogneiss that underlies most of the central Grouse Creek Mountains was dated at 2.51 ± 0.17 Ga based on a 10-point whole-rock Rb-Sr isochron (Compton et al., 1977), but the authors noted significant scatter of data points away from the isochron. To the north in the Albion Range, orthogneiss that forms part of the Precambrian basement complex was dated by the Rb-Sr isochron method at 2.46 Ga by Armstrong and Hills (1967). The orthogneiss in the Grouse Creek Mountains is composed of three main lithologies, which reflect three protoliths of possibly different intrusive age. From oldest to youngest, these are a coarse-grained, biotite orthogneiss, a fine- to coarse-grained leucocratic orthogneiss with abundant muscovite, and a younger leucocratic orthogneiss with up to 20 cm megacrysts of albite (Todd, 1973). All three lithologies are intimately mingled at the regional and outcrop scale in the map area and are also highly deformed, giving rocks the appearance of banded gneiss. Greenschist- to amphibolite-grade metamorphism of the protolith was accompanied by deformation, which resulted in a strong, sub-horizontal foliation and a N-S mineral lineation. As described above, these rocks also host a second, superimposed subhorizontal foliation with an E-W lineation developed at amphibolite-facies conditions.

Sample PCMG is a mafic, biotite-rich lithology in the banded orthogneiss complex (Fig. 2). In plane light, zircons from PCMG appear dark and opaque with a greasy luster, suggesting they might be metaminct and thus difficult to date with precision. In many of these grains, however, CL revealed regular zoning, and it was determined that the greasy appearance was related to incorporation of biotite into the rims of the zircons, probably during one of the several metamorphic events that affected the protolith (Egger, 2001).

SHRIMP analysis supports this conclusion. The zircons define a discordia line with an upper intercept at ~2.62 Ga and a lower intercept at ~160 Ma (Fig. 11). In a few grains, 160 Ma rims were dated that have grown around Archean cores. Although

significant geochronologic work remains to be done on the orthogneiss, these data suggest that an important metamorphic event likely affected the Archean granitoid suite around 160 Ma. This Jurassic age is common for plutons, metamorphism, and deformation in the hinterland of the Sevier thrust belt (D. Miller et al., 1987; E. Miller et al., 1988), but the limited and preliminary nature of these data do not warrant conclusions about the still largely unknown age(s) of pre-Tertiary deformation and metamorphism in the Grouse Creek Mountains.

Geochemistry

The five samples of plutonic rocks dated were also analyzed for major- and trace-element geochemistry using X-ray fluorescence at the Washington State University Geoanalytical Facility. Data are listed in Table 1. This additional information was collected to help assess the role of crustal contamination in the origin of the plutons and its effect on the age and nature of the zircon populations.

All four granitoids are peraluminous (Table 1, A/CNK) with an upper continental crust trace-element signature (Fig. 12A). In the Emigrant Pass plutonic complex, A/CNK values range from 1.03–1.05, and are increasingly peraluminous and increasingly felsic with the passage of time (Table 1). These data, in conjunction with a relatively high initial $^{87}Sr/^{86}Sr$ ratio of 0.709 (Compton et al., 1977) and the presence of garnetiferous aplite dikes, imply a crustal component to the magma. The ratio of Ca content versus Fe, Mg, and Ti (C/FMT) was also plotted (Fig. 12B) to distinguish hybridization of basalt and crustal melt from restite mixing (Patiño-Douce, 1999). Whereas TEP1 and TEP2 fall within the realm of an empirically determined greywacke melt source, TEP3 is clearly a product of some hybridization of basalt and metapelite, as is also suggested by the presence of mafic enclaves investigated in the field.

The Red Butte pluton is strongly peraluminous (A/CNK = 1.12) and has a high initial $^{87}Sr/^{86}Sr$ ratio of 0.714 (Compton et al., 1977). Todd (1980) noted the presence of 0.5% magmatic muscovite in the main phase of the pluton and abundant muscovite and garnet in a late alaskite phase; mafic inclusions are rare. In the C/FMT plot (Fig. 12B), sample TRB plots in the region of overlap between felsic pelite and greywacke melt sources.

Apatite Fission-Track Data

Apatite fission-track data were collected in two E-W transects, one across the Grouse Creek Mountains through the Emigrant Pass plutonic complex, and another across the Albion Mountains (Figs. 1 and 2). The fission-track data were essentially constant in age across the transects, with a weighted mean age of 13.4 Ma, a mean track length of about 14 microns, and with relatively narrow, unimodal track-length distributions (Table 2, Figs. 13 and 14). Such data suggest a short period of rapid exhumation and consequent cooling, with cooling through the 100°C isotherm at about 13 Ma.

The rapid exhumation documented by the fission-track data was likely accommodated by motion along the down-to-the-west Grouse Creek fault (Figs. 2 and 3), which extends N-S along the western flank of the range. In the southern Grouse Creek Mountains, the fault exhibits a range of dips from about 30° W to 20°W, and places Tertiary fanglomerates, breccias, tuffs, tuffaceous sediments, and lacustrine limestones in a hanging-wall position against Archean to Permian strata in the footwall (Compton, 1983). A tuff at the base of the section has been dated at ~34 Ma, and the section is intruded by 11–14 Ma rhyolite plugs (Compton, 1983). The 2 km thick Tertiary stratigraphic succession deposited in a hanging-wall position suggests a minimum 2 km vertical (stratigraphic) throw on this fault. The pre-faulting thickness of older units involved in the faulting is not precisely known in this region, and this displacement could be several km greater. On the eastern side of the range, high-angle normal faults also bound the Grouse Creek Mountains (Fig. 2). Quaternary alluvium covers these faults locally, but gravity data suggest that the Quaternary cover is <500 m thick (Cook et al., 1964), implying that offset along these faults is less than those that bound the range on its west side.

In the Albion Mountains, the range-bounding fault is inferred, but has not been mapped, along the western range front. Again, a lesser offset normal fault has been mapped along the eastern side of Middle Mountain. This fault bounds the valley between Middle Mountain and the Albion Range, and has an offset of less than 1 km (Stanford Geological Survey, unpubl. data, 1991).

Figure 13 compares the results of fission track data from the Albion and Grouse Creek Mountains (this paper) with that reported from the Raft River Mountains by Wells et al. (2000). Fission-track ages

TABLE 1. Major and Minor Element Geochemistry

Sample:	TRB	TEP1	TEP2	TEP3	PCMG
Latitude:	41°40'25"	41°30'15"	41°32'10"	41°30'50"	41°40'25"
Longitude:	113°45'10"	113°38'20"	113°45'20"	113°45'00"	113°44'50"
Age, Ma	25.3 ± 0.5 Ma	34.3 ± 0.3 Ma	36.1 ± 0.2 Ma	41.3 ± 0.3 Ma	~2.62 Ga
			Normalized results, wt %		
SiO_2	75.09	74.39	72.63	70.06	67.04
Al_2O_3	14.00	14.07	14.93	15.61	17.00
TiO_2	0.133	0.200	0.231	0.394	0.552
FeO*	1.23	1.47	1.78	2.79	3.83
MnO	0.045	0.038	0.053	0.060	0.037
CaO	0.78	1.84	1.97	3.03	4.05
MgO	0.25	0.48	0.47	1.04	1.24
K_2O	5.04	3.96	3.87	3.08	2.01
Na_2O	3.39	3.50	4.00	3.83	4.05
P_2O_5	0.038	0.057	0.072	0.108	0.175
A/CNK	1.12	1.05	1.04	1.03	1.05
			Trace elements, ppm		
Ni	17	15	20	22	20
Cr	4	2	7	13	17
Sc	7	6	3	8	11
V	12	17	24	42	42
Ba	417	703	738	781	1057
Rb	255	173	144	102	117
Sr	72	175	202	255	248
Zr	101	95	115	139	329
Y	37	13	26	14	13
Nb	36.7	14.6	24.1	13.5	14.0
Ga	25	18	16	18	22
Cu	4	3	0	3	16
Zn	72	37	40	44	83
Pb	53	45	46	24	17
La	18	14	40	46	90
Ce	58	26	72	72	138
Th	20	13	23	15	32

[1]Major elements are normalized on a volatile-free basis, with total Fe expressed as FeO. XRF geochemical analysis was performed at Washington State University.

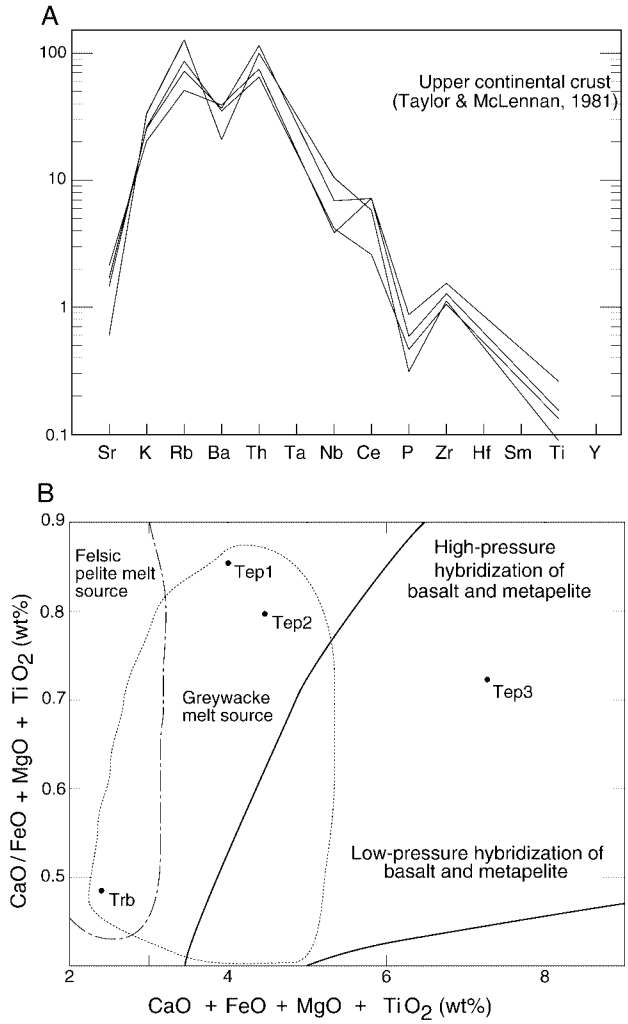

FIG. 12. A. Trace-element spider diagram. Data are normalized to the MORB values of Pearce (1983) and mimic upper continental crust trace-element signature. B. C/FMT plot distinguishes hybridization from pure crustal melt (after Patiño-Douce, 1999). Data suggest earliest intrusion (TEP3) represents hybridization of basalt with crust, whereas subsequent intrusions contain a larger component of crust. TRB appears to have a different source than any of the TEP samples.

from the Raft River Mountains show a pattern of younging to the east, from ages similar to those reported here on the western side of the range to a youngest reported age of 7.4 Ma on the eastern end of the range.

Discussion

The data presented here help us address questions about the specific timing and nature of magmatism, metamorphism, and extension in the Grouse Creek–Albion–Raft River metamorphic core complex. Distinguishing Cenozoic from Mesozoic events has been a long-standing problem in this region. Our data allow us to more clearly place age limits on which events are Cenozoic in age and associated with various stages of extensional deformation in this part of the Basin and Range province. At least three discrete episodes of extension-related deformation are represented in the Grouse Creek Moun-

TABLE 2. Fission-Track Sample Locality, Counting, and Age Data[1]

Sample no.	Irradiation no.	Latitute, °N	Longitude, °W	No. xls	Spontaneous		Induced		P(_)[2], %	Dosimeter		Age, ± 2 Ma Ma
					Rho-S	NS	Rho-I	NI		Rho-D	ND	
Samples analyzed by C. Savage												
GG1	SU003-06	42° 08' 58"	113° 50' 49"	20	0.1266	235	3.946	7326	52	1.729	6713	11.1 ± 1.5
GG2	SU003-17	42° 08' 25"	113° 50' 19"	20	0.0574	106	1.499	2769	63	1.713	6653	13.1 ± 2.6
GG4	SU003-07	42° 08' 27"	113° 49' 38"	20	0.0497	68	1.010	1383	64	1.727	6713	16.9 ± 4.2
KG1	SU003-15	42° 08' 59"	113° 47' 51"	20	0.0599	53	1.576	1394	<0.1	1.715	6653	13.0 ± 3.6
91AL-E-29	SU003-18	42° 11' 24"	113° 47' 39"	20	0.0237	30	0.882	1119	35	1.712	6653	9.2 ± 3.4
C914F	SU003-20	42° 05' 45"	113° 41' 59"	20	0.0655	121	1.528	2823	62	1.710	6653	14.6 ± 2.7
DMS160	SU003-19	42° 07' 02"	113° 37' 55"	20	0.0261	25	0.831	795	23	1.711	6653	10.7 ± 4.4
Samples analyzed by T. Dumitru												
GG1[2]	SU008-15	42° 08' 58"	113° 50' 49"	30	0.1829	414	4.150	9391	11	1.508	4261	12.8 ± 1.3
C914F[2]	SU008-17	42° 05' 45"	113° 41' 59"	16	0.1060	164	2.055	3180	9	1.519	4261	15.1 ± 2.4
91AL-E-7[2]	SU008-16	42° 07' 05"	113° 43' 51"	26	0.2191	541	3.855	9519	62	1.513	4261	16.6 ± 1.6
Tep9	SU007-21	41° 32' 13"	113° 46' 04"	15	0.2023	105	4.708	2444	4.3	1.557	4525	12.1 ± 3.4
Tep7	SU007-19	41° 30' 33"	113° 38' 27"	15	0.0751	46	1.553	951	53	1.561	4525	14.6 ± 4.4
95BR156[3]	SU031-26	41° 30' 17"	113° 38' 24"	40	0.1250	395	2.927	9246	5.4	1.598	4818	13.2 ± 1.4
95BR153re[3]	SU031-23	41° 32' 05"	113° 45' 26"	35	0.1979	334	4.701	7933	22	1.631	4818	13.2 ± 1.5
95BR155[3]	SU031-25	41° 30' 59"	113° 39' 23"	36	0.1600	439	3.508	9627	69	1.609	4818	14.1 ± 1.4
95BR154re[3]	SU031-24	41° 32' 11"	113° 45' 58"	31	0.1609	183	3.990	4538	37	1.609	4818	12.5 ± 1.9

[1]Abbreviations are: No xls = number of individual crystals (grains) dated; Rho-S = spontaneous track density (x 10^6 tracks per cm^2); NS = number of spontaneous tracks counted; Rho-I = induced track density in external detector (muscovite) (x 10^6 tracks per cm^2); NI = number of induced tracks counted; P(_^{2}),[2] = probability (Galbraith, 1981; Green, 1981); Rho-D = induced track density in external detector adjacent to dosimetry glass (x 10^6 tracks per square centimeter); ND = number of tracks counted in determining Rho-D; Age = sample pooled fission-track age (Green, 1981) calculated using zeta calibration method (Hurford and Green, 1983). The following is a summary of key laboratory procedures. Savage analyzed seven samples as part of his Stanford University undergraduate honors thesis (Savage, 1992). Dumitru reanalyzed two of these samples as well as seven additional samples. Apatites were etched for 20 s in 5N nitric acid at room temperature. Grains were dated by external detector method with muscovite detectors. Samples were irradiated in well thermalized positions of Texas A&M University (SU003, SU007, SU008) or Oregon State University (SU031) reactor. CN5 dosimetry glasses with muscovite external detectors were used as neutron flux monitors. External detectors were etched in 48% HF. Tracks counted with Zeiss Axioskop microscope with 100× air objective, 1.25× tube factor, 10× eyepieces, transmitted light with supplementary reflected light as needed; external detector prints were located with Kinetek automated scanning stage (Dumitru, 1993). Only grains with c axes subparallel to slide plane were dated. Ages calculated using zeta calibration factor of 399.7 for CS or 385.9 for TD. Confined tracks lengths were measured on seven of the samples. Lengths were measured only in apatite grains with c axes subparallel to slide plane; only horizontal tracks were measured (within ±5–10°), following protocols of Laslett et al.(1982). Lengths were measured with computer digitizing tablet and drawing tube, calibrated against stage micrometer (Dumitru, 1993). Age calculations were done with program by D. Coyle.

[2]Track length data collected from separate ^{252}Cf exposed slide (Donelick and Miller, 1991) and shown in Figure 14.

[3]Track length data collected from same slide used for age analysis and shown in Figure 14.

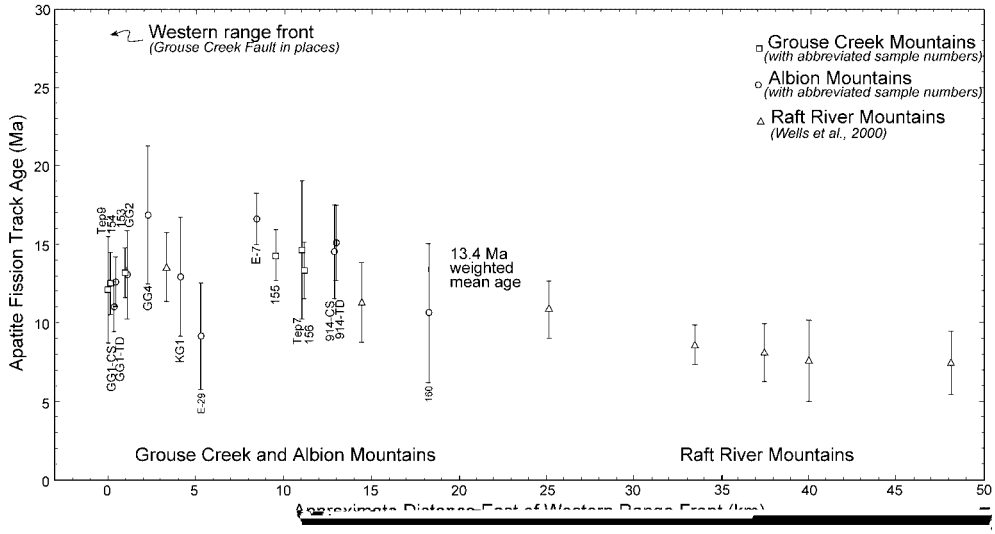

FIG. 13. Apatite fission-track data from the Grouse Creek–Albion–Raft River metamorphic core complex. Data from the western ranges center around a mean age of 13.4 Ma, indicating that cooling through 100°C was synchronous throughout the length of the complex in a N-S direction. This likely reflects the onset of Basin and Range–related extension along range-bounding normal faults, such as the Grouse Creek fault. Younger ages in the Raft River Mountains to the east probably represent late Miocene unroofing associated with E-directed detachment faulting (Wells et al., 2000). Earlier, Compton et al. (1977), reported apatite fission-track ages of 18.9 ± 6.3 Ma and 13.7 ±3.7 Ma from the Red Butte pluton.

tains, separated by 15 m.y. Faulting associated with Basin and Range development is a fourth event and post-dates these events by another 10 m.y. Each of these extensional events is discussed separately, followed by comments on their relevance to events in the core complex as a whole.

Pre–41 Ma extension

In the Grouse Creek Mountains, a pre–41 Ma extensional event produced a series of faults that omit structural and stratigraphic section. The western phase of the Emigrant Pass pluton intrudes these faults at shallow levels in the crust at 41 Ma (Fig. 2), providing an upper age bracket for the faulting. Across the Albion–Raft River–Grouse Creek metamorphic core complex, there is everywhere evidence for faults that omit section, but nowhere are they directly dated. In many places such as here in the Grouse Creek Mountains, they are overprinted by younger deformation and, in most cases, often metamorphosed as well.

Syn–36–34 Ma folding

Intrusion of the western and eastern phases of the pluton at 36 and 34 Ma is associated with large-scale folding of the faults and country rocks adjacent to and above the pluton (Figs. 2 and 3). The relations described in this paper are used to assign an Oligocene age to the formation of the Bovine Mounain recumbent fold. The easiest explanation for this fold is that rock units were tilted E or W about a N-S axis during earlier faulting, and that intrusion of the plutons heated roof rocks that shortened vertically, producing a N-S–trending fold with a subhorizontal axial plane. Final depth of intrusion is believed to have been no greater than 5–10 km, based on the thickness of stratigraphic overburden and metamorphic assemblages developed in the contact aureole of the plutons. Thus, over an 8 m.y. time span, the Emigrant Pass plutonic complex heated successively higher levels of the crust, ultimately promoting formation of the map-scale, recumbent Bovine fold and associated subhorizonal cleavage during the final phase of intrusion. The increasingly felsic and peraluminous nature of the series of intrusions that make up the Emigrant Pass plutonic complex suggests that this composite pluton is a product of hybridization of mantle-derived basalt with increasing amounts of crustal melt (Fig. 12B). The presence of inherited zircon cores in the

final phase of intrusion implies that the amount of crustal melt derived from an upper crustal source and incorporated into this magma was significant and increased with time.

Early Miocene extension

The pre-41 Ma extensional event and the metamorphism and deformation of upper crustal levels as documented by the Bovine fold was followed by a third and younger extension-related event at least 15 m.y. later in the early Miocene. During this younger event, the Emigrant Pass pluton and its

including the Emigrant Pass pluton, is unaffected by this younger metamorphic and deformational event, providing additional evidence that the Ingham Pass fault separates the two regions into an upper (south part of the range) and lower plate across this fault (Fig. 2; Egger, 2001). Thus, exposures of the Miocene upper crust are represented by rocks in the southern Grouse Creek Mountains.

Unlike the Emigrant Pass pluton, there is no geologic evidence for a more mafic component to the magmas of the Red Butte pluton, yet the evidently large crustal component to the melt (as seen by its peraluminous nature and high proportion of inherited cores in the zircons) and its wide metamorphic aureole would be difficult to achieve in the middle to upper crust without continued addition of mantle-derived magmas and heat to the crust. In addition, a pluton sourced from a pure crustal melt would have an A/CNK value >1.2 (Patiño-Douce, 1999), significantly higher than the measured value of 1.12 for the Red Butte pluton. Granites emplaced in continental settings that have large crustal components to their magmas are often thought to be the result of decompression melting, caused by the collapse of previously overthickened crust (Patiño-Douce, 1999). If gravitational collapse were a major driving force behind extension in the Grouse Creek region, then extension should directly follow shortening. Instead, we see a 50 m.y. time lapse between the accepted end of thrust faulting in the foreland at 70–80 Ma (e.g., DeCelles, 1994) and the onset of extensional deformation localized during intrusion of the Red Butte pluton at 25 Ma. Although the location of the Grouse Creek Mountains corresponds to a region of the crust that underwent crustal thickening during the Sevier and Laramide orogenies (e.g., Coney, 1980), decompression melting cannot explain the origin of the Red Butte pluton. Instead, the introduction of heat into middle levels of the crust through magmatic heating and the melting of crust most likely led to the final diapiric rise of the Red Butte pluton and its country rocks through the crust. Thus, extension in this part of the Grouse Creek Mountains appears driven by, and most certainly localized by, magmatism.

Late Miocene extension

A final episode of late Miocene extension exhumed the present Grouse Creek Mountains along N-S–oriented range-bounding normal faults. The episode of major motion along these faults is constrained by consistent apatite fission-track ages at ~13.4 Ma in the Grouse Creek and Albion Mountains. Normal faults bound both sides of the Grouse Creek Mountains (Fig. 2), but far greater offset is seen on the fault along the western side of the range than on the eastern side. The down-to-the-west Grouse Creek fault places Miocene sedimentary rocks on Archean–Permian rocks in the footwall and, based on the thickness of the Tertiary succession, represents a minimum of 2 km of stratigraphic throw. By inference, motion along the 25 Ma Ingham Pass fault, together with diapiric rise of lower-plate rocks, must have been complete by the time Basin and Range faulting began, inasmuch as the Emigrant Pass plutonic complex and Red Butte pluton were equally uplifted and exhumed at the same time by the range-bounding Grouse Creek fault (Figs. 1 and 2). Although constraints on the location and offset of range-bounding faults in the Albion Range to the north are poor, apatite fission-track data indicate that the Grouse Creek Mountains appear to have behaved as a single crustal block together with the western Raft River and Albion Mountains during faulting and exhumation in the late Miocene. Rhyolite plugs dated at 11.4 Ma southwest of the Grouse Creek Mountains are inferred to largely post-date extension (Compton, 1983) and also suggest that magmatism continued intermittently in this region, into the time span of motion of the major range-bounding faults.

Conclusions: Relationship of Events in the Grouse Creek Mountains to Events in the Greater Raft River–Grouse Creek Metamorphic Core Complex

Multiple Tertiary deformational events are recognized throughout the Grouse Creek–Albion–Raft River metamorphic core complex; in some areas, they can be demonstrated to have been superimposed upon an earlier, probably Mesozoic, deformational history. Although all parts of the complex have a complicated Tertiary history in common, the exact timing and nature of events appears to vary, dependent on existing age constraints and/or interpretations thereof (Fig. 15). Here we compare events as reported from the Raft River Mountains to those discussed in this paper, mainly from the Grouse Creek Mountains.

In the Raft River Mountains (Fig. 1), Wells et al. (2000) reported three periods of rapid cooling as recorded in $^{40}Ar/^{39}Ar$ ages of biotite, muscovite, and K-feldspar and apatite and zircon fission-track ages.

The first is in the Eocene, recorded by muscovite $^{40}Ar/^{39}Ar$ ages of ~47 Ma and biotite ages of ~45 Ma. They interpreted this cooling to result from top-to-the-WNW motion along the Middle Mountain shear zone (MMSZ) (Saltzer and Hodges, 1988; Wells et al., 1997b). They believed that this Eocene event continued as late as 37 Ma in the western Raft River Mountains, based on the youngest cooling ages obtained from muscovite from mylonitized rocks (Wells et al., 1997b). A second period of rapid cooling was suggested to be recorded by $^{40}Ar/^{39}Ar$ ages that span the latest Oligocene and early Miocene, from about 25–20 Ma (Wells et al., 2000). This cooling was postulated to be related to continued top-to-the-west motion along the MMSZ, or to the initiation of motion along the top-to-the-east Raft River detachment (Fig. 1). Finally, a middle- to late Miocene event is recorded in apatite fission-track ages that young progressively to the east from 13.5 Ma in the westernmost part of the range to 7.4 Ma in the east (Fig. 13). These ages are interpreted to reflect footwall exhumation by the top-to-the-east Raft River detachment. Because there are no known Tertiary plutons exposed in the Raft River Mountains, these multiple exhumation/extensional events possibly took place in the absence of contemporaneous magmatism, at least at presently exposed crustal levels.

A comparison of these proposed histories (Fig. 15) suggests that the Grouse Creek Mountains may also provide evidence for Tertiary faulting and exhumation (cooling) of rocks in the Eocene. Data presented in this paper from the southern Grouse Creek Mountains provide definitive evidence for normal faults that are cut by the 41 Ma phase of the Emigrant Pass plutonic complex. There is no lower age bracket on this event. The SHRIMP zircon ages presented here revise the 38 Ma Rb-Sr isochron age for the westernmost phase of the Emigrant Pass plutonic complex presented by Compton et al. (1977), and provide a slightly earlier upper age bracket for pre-intrusive faulting. Greenschist-facies metamorphism, cleavage development, and generation of a map-scale recumbent fold beneath Bovine Mountain in the southern Grouse Creek Mountains is interpreted here to be synchronous with emplacement of the younger phases of the Emigrant Pass plutonic complex at 34–36 Ma. Metamorphic mineral assemblages and stratigraphic depths indicate that the Emigrant Pass plutonic complex was emplaced at depths less than 5–10 km. The Emigrant Pass plutonic complex was clearly responsible for transferring heat to shallow, once brittle levels of the crust,

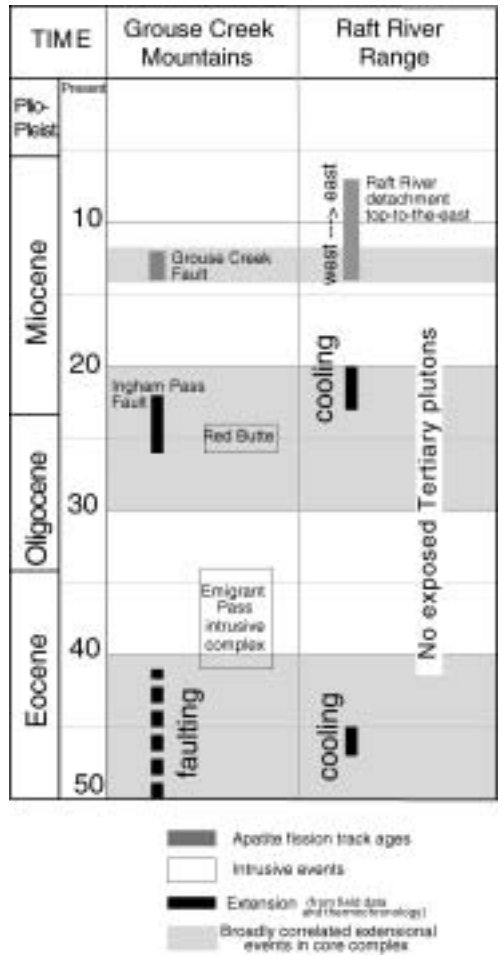

FIG. 15. Summary of the timing of plutonism and extension; comparison of data from the Grouse Creek Mountains to the Raft River Mountains. See text for specific ages, techniques, and references.

and localizing ductile deformation of roof and country rocks during the Oligocene.

The second period of rapid cooling postulated by Wells et al. (2000) in the Raft River Mountains may correspond to deformation associated with intrusion of the Red Butte Pluton at 25 Ma in the Grouse Creek Mountains and, together, may indicate that an important episode of deformation, intrusion, and exhumation of lower-plate basement complex rocks occurred in the Miocene. Metamorphic and field relations in the Grouse Creek Mountains documented by Todd (1973, 1980) indicate that country rocks adjacent to the Red Butte pluton were meta-

morphosed at depths of 15–20 km and were remobilized, rising diapirically during intrusion of the Red Butte pluton. This paper reports normal-sense motion along the Ingham Pass fault during this event, and identifies this structure as a major crustal-penetrating fault zone that juxtaposed what were once deep crustal levels in the Miocene with upper crustal levels represented by exposures of rocks in the upper plate of this fault in the southern Grouse Creek Mountains (Fig. 2).

Fission track data from as far south as the Emigrant Pass pluton and as far north as the Albion Mountains suggest final cooling and exhumation of the western part of the larger Grouse Creek–Raft River–Albion Mountains metamorphic core complex at about 13.4 Ma. The fault that was responsible for this uplift in the Grouse Creek Range is the Grouse Creek fault. As this fault moved, about 2 km of sedimentary fill accumulated along the western side of the Grouse Creek Mountains. The succession is dated at its base as 34 Ma based on ages of rhyolite tuff, and the Tertiary succession is cut by rhyolite plugs and domes dated at 14–11 Ma (Compton, 1983), providing a record of continuing magmatism in this region up to the time of Basin and Range faulting.

What appears to be a short period of rapid exhumation in the Grouse Creek and Albion Mountains at 13 Ma appears to mark just the beginning of a longer faulting and exhumation event in the Raft River Mountains. Fission track ages reported by Wells et al. (2000) young to the east, which they interpreted as a protracted period of west-to-east exhumation lasting as long as 6 m.y. (Fig. 13), from about 13.5 Ma to 7.4 Ma. These data are consistent with our conclusions, but our data provide additional evidence that the core complex was exhumed bi-directionally along two faults: the down-to-the-west Grouse Creek fault on the western side of the range and the down-to-the-east Raft River detachment on the eastern side of the range (Fig. 1; Mallavielle, 1987a, 1987b).

In conclusion, the results of geologic mapping and geochronology/thermochronology reported here suggest a protracted history of magmatism and extension-related deformation in the Grouse Creek Mountains, which form just the southern part of the larger Albion–Raft River–Grouse metamorphic core complex. This history of extension-related deformation and magmatism began prior to 41 Ma and continued to 11 Ma spanning at least 30 m.y. of time. It is unclear at present if events documented in the Grouse Creek Mountains correlate exactly to events elsewhere in the complex. Specifically, no Tertiary plutons are present in the Raft River Mountains and events are defined by cooling histories (e.g., Wells et al., 2000). The geology of the Grouse Creek Mountains provides a good example of changing relations between magmatism and extensional deformation at two very different levels of the crust, represented by rocks in the upper plate versus lower plate of the Ingham Pass fault. Relations at higher structural levels indicate that magmatism can transport heat to upper levels of the crust; rising temperatures through time allow rocks that once underwent faulting in the brittle crust to deform ductilely in a metamorphic environment. At deeper levels of the crust, deformation of country rocks is pervasive and entirely ductile in nature, localized/enhanced by the emplacement of granitoid plutons. Syn-extensional plutons can diapirically rise through the crust, entraining their deforming country rocks, and ultimately must become partially deformed themselves as they are uplifted into the brittle regime by faults such as the Ingham Pass fault.

Acknowledgments

This work was made possible through grants awarded to Anne E. Egger by ARCO and the Stanford University McGee Fund. Mapping was funded by USGS EDMAP Grant # 00HQAG0062 awarded to Anne E. Egger and Cynthia M. Martinez. The authors acknowledge helpful review comments from Peter Copeland, Michael Wells, David Foster, and an anonymous reviewer.

REFERENCES

Anderson, J. L., 1988, Core complexes of the Mojave-Sonoran desert: Conditions of plutonism, mylonitization, and decompression, *in* Ernst, W. G., ed., Metamorphism and crustal evolution of the Western United States. Rubey Volume VII: Englewood Cliffs, NJ: Prentice-Hall, p. 502–525.

Armstrong, R. L., 1970, Geochronology of Tertiary igneous rocks, eastern Basin and Range province, western Utah, eastern Nevada, and vicinity, USA: Geochimica et Cosmichimia Acta, v. 34, p. 203–232.

Armstrong, R. L., and Hills, F. A., 1967, Rb-Sr and K-Ar geochronologic studies of mantled gneiss domes, Albion Range, southern Idaho, USA: Earth and Planetary Science Letters, v. 3, p. 114–124.

Baker, W. H., 1959, Geologic setting and origin of the Grouse Creek pluton, Box Elder County, Utah: Unpubl. Ph.D. thesis, University of Utah.

Brun, J. P., Sokoutis, D., and Driessche, J. V. D., 1994, Analogue modeling of detachment fault systems and core complexes: Geology, v. 22, p. 319–322.

Buck, W. R., 1988, Flexural rotation of normal faults: Tectonics, v. 7, p. 959–973.

Compton, R. R., 1972, Geologic map of the Yost quadrangle, Box Elder County, Utah, and Cassia County, Idaho: USGS Miscellaneous Geologic Investigations, Map I-672.

_____, 1975, Geologic map of the Park Valley quadrangle, Box Elder County, Utah, and Cassia County, Idaho: USGS Miscellaneous Geologic Investigations, Map I-873.

_____, 1983, Displaced rocks on the west flank of the Raft River–Grouse Creek core complex, Utah: Geological Society of America Memoir 157, p. 271–279.

Compton, R. R., Todd, V. R., Zartman, R. E., and Naeser, C. W., 1977, Oligocene and Miocene metamorphism, folding, and low-angle faulting in northwestern Utah: Geological Society of America Bulletin, v. 88, p. 1237–1250.

Cook, K. L., Halverson, M. O., Stepp, J. C., and Berg, J. W., 1964, Regional gravity survey of the northern Great Salt Lake Desert and adjacent areas in Utah, Nevada, and Idaho: Geological Society of America Bulletin, v. 75, no. 8, p. 715–740.

Coney, P. J., 1980, Cordilleran metamorphic core complexes: An overview: Geological Society of America Memoir 153, p. 7–31.

DeCelles, P. G., 1994, Late Cretaceous–Paleocene synorogenic sedimentation and kinematic history of the Sevier thrust belt, northeast Utah and southwest Wyoming: Geological Society of America Bulletin, v. 106, p. 32–56.

Donelick, R. A. and Miller, D. S., 1991, Enhanced TINT fission track densities in low spontaneous track density apatites using ^{252}Cf-derived fission fragment tracks: A model and experimental observations: Nuclear Tracks and Radiation Measurements, v. 18, pp. 301–307.

Dumitru, T. A., 1993, A new computer-automated microscope stage system for fission track analysis: Nuclear Tracks and Radiation Measurements, v. 21, p. 575–580.

_____, 2000, Fission-track geochronology, *in* Noller, J. S., Sowers, J. M., and Lettis, W. R., eds., Quaternary geochronology: Methods and applications: American Geophysical Union Reference Shelf, v. 4, p. 131–156.

Egger, A. E., 2001, Magmatism and extension in the Grouse Creek Mountains, Utah: Evolution of a metamorphic core complex: Unpubl. M.S. thesis, Stanford University, 40 p. and plates.

_____, 2003a, Geologic map of the Emigrant Pass 7.5' quadrangle, Box Elder County, Utah: Utah Geological Survey Open File Report, submitted.

_____, 2003b, Geologic map of the Potters Creek 7.5' quadrangle, Box Elder County, Utah: Utah Geological Survey Open File Report, submitted..

Egger, A. E., Miller, E. L., and Dumitru, T. A., 2000, Multiple episodes of Tertiary extension and intrusion in the Grouse Creek–Albion–Raft River metamorphic core complex, Utah-Idaho: Geological Society of America Abstracts, v. 32, no. 7, p. 44.

Forrest, S. E., Miller, E. L., and Wright, J. E., 1994, Oligocene plutonism and associated crustal thinning in the southern Albion Mountains, Idaho: Geological Society of America Abstracts, v. 26, no. 7, p. 192.

Galbraith, R. F., 1981, On statistical models for fission track counts: Mathematical Geology, v. 13, p. 471–478.

Green, P. F., 1981, A new look at statistics in fission-track dating: Nuclear Tracks and Radiation Measurements, v. 5, p. 77–86.

Greenwood, H. J., 1967, Wollastonite stability in H_2O-CO_2 mixtures and occurrence in a conact metamorphic aureole near Salmo, British Columbia, Canada: American Mineralogist, v. 52, p. 1669–1668.

Hurford, A. J., and Green, P. F., 1983, The zeta age calibration of fission-track dating: Chemical Geology, v. 41, p. 285–317.

Jordan, T. E., 1983, Structural geometry and sequence, Bovine Mountain, northwestern Utah: Geological Society of America Memoir 157, p. 215–228.

Laslett, G. M., Kendall, W. S., Gleadow, A. J. W., and Duddy, I. R., 1982, Bias in the measurement of fission track length distributions: Nuclear Tracks and Radiation Measurements, v. 6, p. 79–85.

Lister, G. S. and Baldwin, S. L., 1993, Plutonism and the origin of metamorphic core complexes: Geology, v. 21, no. 7, p. 607–610.

Malavielle, J., 1987a, Extensional shearing and km-scale "a" type folds in a Cordilleran metamorphic core complex (Raft River Mountains, northwest Utah): Tectonics, v. 6, p. 423–445.

_____, 1987b, Kinematics of compressional and extensional ductile shearing deformation in a metamorphic core complex of the northeastern Basin and Range: Journal of Structural Geology, v. 9, no. 5, p. 541–554.

Martinez, C. M., in progress, Geologic map of the Bovine 7.5' quadrangle, Box Elder County, Utah: Utah Geological Survey Open File Report.

Martinez, C. M., and Egger, A. E., in progress, Geologic map of the Rocky Pass Peak 7.5' quadrangle, Box Elder County, Utah: Utah Geological Survey Open File Report.

McCarthy, J., and Brown, L. L., 1986, Reflection profiles from the Snake Range metamorphic core complex, a window into the mid-crust, *in* International Symposium on Deep Structure of the Continental Crust:

Results from reflection seismology: Ithaca, NY, p. 281–292.

Miller, D. M., 1980, Structural geology of the northern Albion Mountains, south-central Idaho: Geological Society of America Memoir 153, p. 399–423.

Miller, D. M., and Bedford, D. R., 1998, Pluton intrusion styles, roof subsidence and stoping, and timing of extensional shear zones in the City of Rocks National Reserve, Albion Mountains, southern Idaho: Utah Geological Association Publication 27, p. 11–25.

Miller, D. M., Hillhouse, W. C., Zartman, R. E., and Lanphere, M. A., 1987, Geochronology of intrusive and metamorphic rocks in the Pilot Range, Utah and Nevada, and comparison with regional patterns: Geological Society of America Bulletin, v. 99, p. 880–885.

Miller, D. M., Nakata, J. K., and Glick, L. L., 1990, K-Ar ages of Jurassic to Tertiary plutonic and metamorphic rocks, northwestern Utah and northeastern Nevada: U.S. Geological Survey Bulletin 1906.

Miller, E. L., Gans, P. B., Wright, J.E., and Sutter, J. F., 1988, Metamorphic history of east-central Basin and Range province, *in* Ernst, W.G., ed., Metamorphism and crustal evolution of the Western United States. Rubey Volume VII: Englewood Cliffs, NJ, Prentice Hall, p. 649–682.

Miller, E. L., Dumitru, T. A., Brown, R. W., and Gans, P. B., 1999, Rapid Miocene slip on the Snake Range–Deep Creek Range fault system, east-central Nevada: Geological Society of America Bulletin, v. 111, no. 6, p. 886–905.

Patiño-Douce, A. E., 1999, What do experiments tell us about the relative contributions of crust and mantle to the origin of granitic magmas?, *in* Castro, A., Fernandez, C., and Vigneresse, J. L., eds., Understanding granites: Integrating new and classical techniques: Geological Society Special Publication 168, p. 55–75.

Pearce, J. A, 1983, Role of the sub-continental lithosphere in magma genesis at active continental margins, *in* Hawkesworth, C. J., and Norry, M. J., eds, Continental basalts and mantle xenoliths: Nantwich, UK: Shiva, p. 230–249.

Saltzer, K. V., and Hodges, S. D., 1988, The Middle Mountain shear zone, southern Idaho: Kinematic analysis of an early Tertiary high-temperature detachment: Geological Society of America Bulletin, v. 100, no. 1, p. 96–103.

Savage, C. F. I., 1992, Fission track dating of Cenozoic uplift in the Albion Mountains, Idaho: Unpubl. B.S. honors thesis, Stanford University, Stanford, California, 21 p.

Spear, F. S., and Cheney, J. T., 1989, A petrogenetic grid for pelitic schists in the system SiO_2-Al_2O_3-FeO-MgO-K_2O-H_2O: Contributions to Mineralogy and Petrology, v. 101, p. 149–164.

Todd, V. R., 1973, Structure and petrology of metamorphosed rocks in central Grouse Creek Mountains, Box Elder County, Utah: Unpubl. PhD thesis, Stanford University, 316 p.

_____, 1980, Structure and petrology of a Tertiary gneiss complex in northwestern Utah: Geological Society of America Memoir 153, p. 349–383.

Wells, M. L., 1997, Alternating contraction and extension in the hinterlands of orogenic belts: An example from the Raft River Mountains, Utah: Geological Society of America Bulletin, v. 109, no. 1, p. 107–126.

Wells, M. L., Dallmeyer, R. D., and Allmendinger, R. W., 1990, Late Cretaceous extension in the hinterland of the Sevier thrust belt, northwestern Utah and southern Idaho, Geology, v. 18, p. 929–933.

Wells, M. L., Hoisch, T. D., Hanson, L., Struthers, J., and Wolff, E., 1997a, Large magnitude thickening and repeated extensional exhumation in the Raft River, Grouse Creek, and Albion Mountains: Brigham Young University Geological Studies, v. 42, p. 325–340.

Wells, M. L., Hoisch, T. D., Peters, M. T., Miller, D. M., Wolff, E. D., and Hanson, L. M., 1998, The Mahogany Peaks Fault, a Late Cretaceous-Paleocene (?) normal fault in the hinterland of the Sevier Orogen: Journal of Geology, v. 106, no. 5, p. 623–634.

Wells, M. L., Snee, L. W., and Blythe, A. E., 2000, Dating of major normal fault systems using thermochronology: An example from the Raft River detachment, Basin and Range, western United States: Tectonics, v. 105, no. B7, p. 16,303–16,327

Wells, M. L., Struthers, J. S., Snee, L. W., Blythe, A. E., and Miller, D. M., 1997b, Miocene extensional reactivation of an Eocene extensional shear zone, Grouse Creek Mountains, Utah: Geological Society of America Abstracts with Programs, v. 29, no. 7, p. A-162

Wernicke, B. P., 1981, Low-angle normal faults in the Basin and Range Province; nappe tectonics in an extending orogen: Nature, v. 291, no. 5817, p. 645–648.

Appendix. Data Tables

TABLE 1. Major and Minor Element Geochemistry

Sample:	TRB	TEP1	TEP2	TEP3	PCMG
Latitude:	41°40'25"	41°30'15"	41°32'10"	41°30'50"	41°40'25"
Longitude:	113°45'10"	113°38'20"	113°45'20"	113°45'00"	113°44'50"
Age, Ma	25.3 ± 0.5 Ma	34.3 ± 0.3 Ma	36.1 ± 0.2 Ma	41.3 ± 0.3 Ma	~2.62 Ga
			Normalized results, wt %		
SiO_2	75.09	74.39	72.63	70.06	67.04
Al_2O_3	14.00	14.07	14.93	15.61	17.00
TiO_2	0.133	0.200	0.231	0.394	0.552
FeO*	1.23	1.47	1.78	2.79	3.83
MnO	0.045	0.038	0.053	0.060	0.037
CaO	0.78	1.84	1.97	3.03	4.05
MgO	0.25	0.48	0.47	1.04	1.24
K_2O	5.04	3.96	3.87	3.08	2.01
Na_2O	3.39	3.50	4.00	3.83	4.05
P_2O_5	0.038	0.057	0.072	0.108	0.175
A/CNK	1.12	1.05	1.04	1.03	1.05
			Trace elements, ppm		
Ni	17	15	20	22	20
Cr	4	2	7	13	17
Sc	7	6	3	8	11
V	12	17	24	42	42
Ba	417	703	738	781	1057
Rb	255	173	144	102	117
Sr	72	175	202	255	248
Zr	101	95	115	139	329
Y	37	13	26	14	13
Nb	36.7	14.6	24.1	13.5	14.0
Ga	25	18	16	18	22
Cu	4	3	0	3	16
Zn	72	37	40	44	83
Pb	53	45	46	24	17
La	18	14	40	46	90
Ce	58	26	72	72	138
Th	20	13	23	15	32

[1]Major elements are normalized on a volatile-free basis, with total Fe expressed as FeO. XRF geochemical analysis was performed at Washington State University.

TABLE A1. TRB Wetherill Data

Sample	$^{206}Pb/^{238}U$	± 6/38	$^{207}Pb/^{235}U$	± 7/35	$^{207}Pb/^{206}Pb$	± 7/6
Trb-1.1	0.00393	5.00E-05	0.02715	0.00086	0.05007	0.00137
Trb-1.2	0.00352	1.70E-04	0.01356	0.01607	0.02796	0.03294
Trb-2.1	0.14136	2.45E-03	3.11280	0.05574	0.15971	0.00045
Trb-2.2	0.00483	1.00E-04	0.03164	0.00228	0.04755	0.00316
Trb-3.1	0.00439	6.00E-05	0.02829	0.00106	0.04672	0.00155
Trb-4.1	0.00387	7.00E-05	0.02498	0.00125	0.04686	0.00207
Trb-5.1	0.00445	1.40E-04	0.02792	0.00153	0.04556	0.00187
Trb-6.1	0.00392	6.00E-05	0.02448	0.00069	0.04534	0.00101
Trb-8.1	0.00379	1.00E-04	0.02455	0.00189	0.04698	0.00325
Trb-9.1	0.00421	5.00E-05	0.02743	0.00124	0.04730	0.00199
Trb-10.1	0.00394	1.10E-04	0.02646	0.00229	0.04866	0.00381
Trb-11.1	0.00494	9.00E-05	0.02860	0.00158	0.04202	0.00211
Trb-20.1	0.00442	8.00E-05	0.02644	0.00326	0.04338	0.00520
Trb-21.1	0.00434	8.00E-05	0.03113	0.00227	0.05202	0.00353
Trb-22.1	0.00461	6.00E-05	0.03235	0.00337	0.05093	0.00518
Trb-23.1	0.00454	6.00E-05	0.02971	0.00134	0.04749	0.00198
Trb-24.1	0.07251	1.01E-03	1.64930	0.02747	0.16497	0.00124
Trb-25.1	0.00393	1.20E-04	0.02483	0.01089	0.04577	0.01984
Trb-26.1	0.00427	7.00E-05	0.03205	0.00280	0.05449	0.00457
Trb-27.1	0.00402	1.00E-04	0.03024	0.00848	0.05460	0.01509
Trb-28.1	0.00385	8.00E-05	0.03170	0.00594	0.05970	0.01097
Trb-29.1	0.00530	1.20E-04	0.02673	0.00761	0.03656	0.01028
Trb-30.1	0.00375	1.00E-04	0.01721	0.00932	0.03331	0.01790
Trb-31.1	0.00411	5.00E-05	0.02194	0.00270	0.03871	0.00468
Trb-32.1	0.00440	7.00E-05	0.02769	0.00273	0.04563	0.00435
Trb-33.1	0.00506	1.00E-04	0.03215	0.00239	0.04608	0.00319
TRB-34.1c	0.00450	1.50E-04	0.02741	0.00303	0.04416	0.00448
TRB-33.1c	0.00386	1.30E-04	0.02546	0.00160	0.04784	0.00232
TRB-20.1c	0.08295	7.18E-03	1.77060	0.16371	0.15482	0.00365
TRB-18.1c	0.10569	1.45E-03	2.11550	0.03429	0.14517	0.00102
TRB-18a.1c	0.48433	6.50E-03	11.46100	0.16005	0.17163	0.00044
TRB-16.1c	0.07854	1.88E-03	1.83460	0.05003	0.16941	0.00177
TRB-2a.1c	0.34091	7.40E-03	8.11740	0.23081	0.17269	0.00274
TRB-2b.1c	0.16557	2.08E-03	3.59850	0.06136	0.15763	0.00159
TRB-5.1c	0.18239	2.43E-03	4.21080	0.06244	0.16744	0.00085
TRB-29a.1c	0.13364	2.06E-03	2.75270	0.04886	0.14939	0.00106

Table continues

TABLE A1. (*continued*)

Age 6/38	± 6/38	Age 7/35	± age 7/35	Age 7/6	± age 7/6
25.31	0.33	27.20	0.85	198.29	64.69
22.64	1.07	13.68	15.97	0.00	0.00
852.34	13.85	1435.80	13.86	2452.60	4.79
31.04	0.64	31.63	2.25	76.73	150.82
28.25	0.39	28.33	1.05	35.02	77.71
24.87	0.47	25.05	1.24	42.38	102.19
28.59	0.91	27.96	1.51	0.00	0.00
25.20	0.37	24.56	0.69	0.00	0.00
24.39	0.65	24.63	1.88	48.20	157.30
27.06	0.33	27.48	1.23	64.33	97.26
25.38	0.71	26.52	2.26	131.36	174.42
31.74	0.55	28.63	1.56	0.00	0.00
28.43	0.51	26.50	3.23	0.00	0.00
27.92	0.54	31.13	2.24	286.07	162.89
29.63	0.39	32.33	3.32	237.85	236.95
29.18	0.37	29.73	1.32	74.03	96.45
451.26	6.08	989.28	10.58	2507.20	12.72
25.31	0.79	24.90	10.84	0.00	0.00
27.44	0.44	32.03	2.76	391.23	200.19
25.85	0.61	30.25	8.39	395.71	778.98
24.78	0.50	31.69	5.86	592.57	457.88
34.09	0.76	26.78	7.56	0.00	0.00
24.12	0.65	17.33	9.35	0.00	0.00
26.45	0.34	22.04	2.69	0.00	0.00
28.31	0.44	27.74	2.70	0.00	0.00
32.54	0.64	32.13	2.35	6.66	154.18
28.95	0.94	27.45	3.00	0.00	0.00
24.83	0.86	25.52	1.59	91.41	110.96
513.68	42.86	1034.80	61.84	2399.90	40.61
647.68	8.48	1153.90	11.24	2289.80	12.15
2546.10	28.27	2561.40	13.13	2573.60	4.28
487.40	11.23	1057.90	18.08	2551.90	17.63
1891.10	35.69	2244.20	26.04	2583.90	26.69
987.68	11.49	1549.20	13.64	2430.30	17.21
1080.00	13.25	1676.10	12.24	2532.20	8.53
808.61	11.71	1342.80	13.31	2338.90	12.25

TABLE A2. TRB Tera-Wasserburg Data

Sample	$^{207}Pb/^{206}Pb$	± 7/6	$^{238}U/^{206}Pb$	± 38/6	Age 38/6[1]	± age 38/6
Trb-1.1	0.04930	0.00129	254.49	3.3660	25.2	0.3
Trb-1.2	0.08284	0.00365	264.89	6.3279	23.2	0.6
Trb-2.1	0.16037	0.00041	7.07	0.1225	759.5	12.4
Trb-2.2	0.05329	0.00103	205.67	4.1943	31.0	0.6
Trb-3.1	0.05120	0.00120	226.41	3.1058	28.2	0.4
Trb-4.1	0.05162	0.00142	257.11	4.8848	24.9	0.5
Trb-5.1	0.04753	0.00173	224.40	7.1234	28.6	0.9
Trb-6.1	0.04669	0.00081	254.88	3.7831	25.2	0.4
Trb-8.1	0.05384	0.00214	261.50	6.9211	24.4	0.6
Trb-9.1	0.04926	0.00063	237.12	2.8570	27.0	0.3
Trb-10.1	0.05228	0.00253	252.33	7.0338	25.3	0.7
Trb-11.1	0.04968	0.00084	200.63	3.4753	31.9	0.6
Trb-20.1	0.06016	0.00216	221.42	3.7422	28.5	0.5
Trb-21.1	0.06020	0.00214	227.95	4.3816	27.7	0.5
Trb-22.1	0.07341	0.00262	210.84	2.5572	29.5	0.4
Trb-23.1	0.04939	0.00110	219.88	2.7646	29.1	0.4
Trb-24.1	0.16651	0.00120	13.76	0.1918	391.3	5.3
Trb-25.1	0.12536	0.00809	228.53	4.8413	25.3	0.6
Trb-26.1	0.05943	0.00281	232.91	3.6041	27.2	0.4
Trb-27.1	0.08263	0.00519	239.96	3.9181	25.6	0.4
Trb-28.1	0.07871	0.00289	253.29	3.9704	24.4	0.4
Trb-29.1	0.07336	0.00286	179.89	3.3746	34.5	0.7
Trb-30.1	0.08147	0.00351	250.76	4.0622	24.5	0.4
Trb-31.1	0.05127	0.00142	239.41	2.8282	26.7	0.3
Trb-32.1	0.06186	0.00192	222.50	3.3166	28.4	0.4
Trb-33.1	0.05860	0.00125	194.47	3.7586	32.6	0.6

[1]207 corrected.

TABLE A3. TEP1 Wetherill Data

Sample	$^{206}Pb/^{238}U$	± 6/38	$^{207}Pb/^{235}U$	± 7/35	$^{207}Pb/^{206}Pb$	± 7/6
Tep1-1.1	0.00532	6.00E-05	0.03586	0.00078	0.04884	0.00085
Tep1-1.2	0.00477	2.50E-04	0.02260	0.01979	0.03437	0.02981
Tep1-2.1	0.00654	1.10E-04	0.04105	0.00179	0.04551	0.00174
Tep1-3.1	0.00521	1.00E-04	0.03376	0.00119	0.04702	0.00131
Tep1-4.1	0.00521	7.00E-05	0.03380	0.00187	0.04706	0.00243
Tep1-5.1	0.00540	7.00E-05	0.03619	0.00132	0.04859	0.00159
Tep1-6.1	0.00517	8.00E-05	0.03531	0.00141	0.04952	0.00174
Tep1-7.1	0.00550	6.00E-05	0.03559	0.00121	0.04695	0.00145
Tep1-8.1	0.00516	8.00E-05	0.03480	0.00121	0.04892	0.00145
Tep1-9.1	0.00594	7.00E-05	0.03820	0.00086	0.04665	0.00083
Tep1-10.1	0.00566	6.00E-05	0.03628	0.00109	0.04649	0.00122
Tep1-11.1	0.00553	9.00E-05	0.03593	0.00179	0.04716	0.00214
Tep1-12.1	0.00553	7.00E-05	0.03004	0.00359	0.03938	0.00461
Tep1-20.1	0.00524	1.80E-04	0.02340	0.01669	0.03236	0.02291
Tep1-21.1	0.00593	8.00E-05	0.03699	0.00430	0.04524	0.00515
Tep1-22.1	0.00536	1.10E-04	0.04115	0.00884	0.05563	0.01175
Tep1-23.1	0.00579	1.40E-04	0.04142	0.00810	0.05191	0.00992
Tep1-24.1	0.02138	3.20E-04	0.30254	0.00590	0.10261	0.00110
Tep1-25.1	0.00535	8.00E-05	0.03311	0.00364	0.04491	0.00482
Tep1-26.1	0.20705	2.70E-03	5.05090	0.07516	0.17692	0.00101
Tep1-27.1	0.00536	1.30E-04	0.03500	0.00229	0.04732	0.00274
Tep1-28.1	0.00509	8.00E-05	0.03662	0.00288	0.05222	0.00393
Tep1-29.1	0.00547	7.00E-05	0.03381	0.00231	0.04485	0.00293
Tep1-30.1	0.00494	1.20E-04	0.03217	0.00694	0.04724	0.00999
Tep1-31.1	0.00559	9.00E-05	0.03737	0.00515	0.04848	0.00653
Tep1-32.1	0.00547	8.00E-05	0.03644	0.00264	0.04829	0.00335
Tep1-33.1	0.00532	7.00E-05	0.03147	0.00370	0.04286	0.00493
Tep1-34.1	0.00516	7.00E-05	0.03034	0.00434	0.04268	0.00600
TEP1-33.1c	0.25414	1.79E-02	5.71100	0.53545	0.16298	0.00879
TEP1-26.1c	0.17195	2.78E-03	3.47200	0.07115	0.14645	0.00157
TEP1-28.1c	0.07745	1.07E-03	1.05590	0.02258	0.09888	0.00145
TEP1-21.1c	0.30713	3.50E-03	6.75600	0.08170	0.15954	0.00045
TEP1-19.1c	0.04713	7.20E-04	0.60965	0.02060	0.09382	0.00266
TEP1-10.1c	0.17856	2.51E-03	3.37460	0.06011	0.13707	0.00128
TEP1-7.1c	0.32273	6.20E-03	7.22710	0.17818	0.16241	0.00215

Table continues

Table A3. (*continued*)

Age 6/38	± age 6/38	Age 7/35	± age 7/35	Age 7/6	± age 7/6
34.23	0.38	35.77	0.77	140.14	41.22
30.68	1.61	22.70	19.85	0.00	0.00
42.03	0.70	40.85	1.75	0.00	0.00
33.48	0.61	33.71	1.17	50.27	65.24
33.50	0.48	33.76	1.84	52.16	118.95
34.73	0.44	36.10	1.30	127.96	79.00
33.26	0.50	35.24	1.39	172.57	84.38
35.35	0.38	35.51	1.19	46.68	72.18
33.17	0.49	34.74	1.19	144.16	71.31
38.18	0.45	38.07	0.84	31.47	41.78
36.39	0.41	36.19	1.07	23.37	61.47
35.52	0.55	35.84	1.75	57.16	104.65
35.57	0.48	30.06	3.54	0.00	0.00
33.72	1.14	23.48	16.69	0.00	0.00
38.12	0.50	36.89	4.22	0.00	0.00
34.49	0.70	40.94	8.65	437.62	437.61
37.19	0.88	41.21	7.92	281.65	386.65
136.40	2.02	268.38	4.61	1671.80	19.98
34.38	0.49	33.08	3.58	0.00	0.00
1213.10	14.43	1827.90	12.69	2624.20	9.56
34.49	0.83	34.93	2.25	65.65	132.15
32.71	0.50	36.52	2.83	294.86	181.61
35.15	0.46	33.77	2.27	0.00	0.00
31.76	0.76	32.15	6.85	61.26	599.98
35.94	0.60	37.26	5.05	122.86	289.82
35.19	0.48	36.34	2.59	113.34	156.10
34.23	0.47	31.46	3.65	0.00	0.00
33.15	0.47	30.35	4.29	0.00	0.00
1459.80	92.44	1933.00	84.43	2486.80	93.87
1022.80	15.31	1520.90	16.28	2304.80	18.54
480.86	6.40	731.79	11.22	1603.10	27.67
1726.60	17.30	2080.00	10.75	2450.80	4.81
296.88	4.41	483.34	13.08	1504.40	54.51
1059.10	13.74	1498.50	14.05	2190.50	16.32
1803.00	30.31	2139.90	22.23	2480.90	22.47

TABLE A4. TEP1 Tera-Wasserburg Data

Sample	$^{207}Pb/^{206}Pb$	± 7/6	$^{238}U/^{206}Pb$	± 38/6	Age 38/6[1]	± age 38/6
Tep1-1.1	0.04965	0.00068	187.62	2.11	34.1	0.4
Tep1-1.2	0.10484	0.00639	191.19	7.26	31.1	1.2
Tep1-2.1	0.04949	0.00063	152.11	2.54	42.1	0.7
Tep1-3.1	0.04877	0.00073	191.62	3.51	33.5	0.6
Tep1-4.1	0.05049	0.00079	191.11	2.67	33.5	0.5
Tep1-5.1	0.05039	0.00091	184.69	2.32	34.7	0.4
Tep1-6.1	0.05383	0.00099	192.29	2.87	33.1	0.5
Tep1-7.1	0.04969	0.00082	181.25	1.96	35.3	0.4
Tep1-8.1	0.05081	0.00100	193.36	2.83	33.1	0.5
Tep1-9.1	0.04964	0.00045	167.72	1.98	38.2	0.4
Tep1-10.1	0.04858	0.00098	176.17	2.01	36.4	0.4
Tep1-11.1	0.05610	0.00092	178.91	2.76	35.5	0.6
Tep1-12.1	0.13702	0.00137	158.54	1.95	35.9	0.4
Tep1-20.1	0.13639	0.00898	165.97	3.40	34.3	0.8
Tep1-21.1	0.10208	0.00116	156.46	1.84	38.2	0.4
Tep1-22.1	0.08568	0.00288	179.22	2.64	34.1	0.5
Tep1-23.1	0.14389	0.00223	152.53	3.12	37.0	0.8
Tep1-24.1	0.10454	0.00094	46.64	0.70	127.2	1.9
Tep1-25.1	0.05921	0.00102	183.61	2.41	34.5	0.4
Tep1-26.1	0.17779	0.00096	4.82	0.06	1076.8	13.0
Tep1-27.1	0.05868	0.00148	183.74	4.39	34.5	0.8
Tep1-28.1	0.06825	0.00178	192.55	2.82	32.5	0.5
Tep1-29.1	0.05965	0.00138	179.45	2.28	35.2	0.4
Tep1-30.1	0.07599	0.00336	195.09	4.12	31.7	0.7
Tep1-31.1	0.06901	0.00153	174.20	2.61	35.9	0.5
Tep1-32.1	0.05388	0.00087	181.41	2.38	35.1	0.5
Tep1-33.1	0.16742	0.00203	158.27	1.99	34.4	0.4
Tep1-34.1	0.10303	0.00283	179.18	2.28	33.3	0.4

[1]207 corrected.

TABLE A5. TEP2 Tera-Wasserburg Data

Sample	$^{207}Pb/^{206}Pb$	± 7/6	$^{238}U/^{206}Pb$	± 38/6	Age 38/6[1]	± age 38/6
Tep2-1.1	0.04964	0.00061	173.18	3.60	37.0	0.8
Tep2-2.1	0.04964	0.00054	179.15	2.34	35.8	0.5
Tep2-3.1	0.04820	0.00075	164.09	2.44	39.1	0.6
Tep2-4.1	0.04975	0.00096	162.00	2.78	39.5	0.7
Tep2-5.1	0.05213	0.00055	175.69	2.95	36.3	0.6
Tep2-6.1	0.05056	0.00133	184.20	2.96	34.7	0.6
Tep2-7.1	0.04820	0.00050	174.19	3.74	36.8	0.8
Tep2-8.1	0.04726	0.00039	165.55	1.93	38.8	0.4
Tep2-9.1	0.16512	0.00177	137.57	1.73	39.7	0.5
Tep2-10.1	0.05010	0.00085	176.69	1.99	36.2	0.4
Tep2-11.1	0.05040	0.00137	173.61	2.20	36.8	0.5
Tep2-11.2	0.05615	0.00153	169.19	2.40	37.5	0.5
Tep2-20.1	0.06073	0.00123	164.98	1.99	38.3	0.5
Tep2-21.1	0.06556	0.00197	167.05	2.38	37.6	0.5
Tep2-22.1	0.06382	0.00256	175.17	2.55	35.9	0.5
Tep2-23.1	0.06390	0.00180	173.89	3.66	36.2	0.8
Tep2-24.1	0.06596	0.00190	175.94	2.58	35.7	0.5
Tep2-25.1	0.07149	0.00342	177.73	2.42	35.0	0.5
Tep2-25.1	0.06536	0.00209	165.54	2.19	37.9	0.5
Tep2-27.1	0.11281	0.00352	181.49	2.35	32.5	0.4
Tep2-28.1	0.05868	0.00120	177.03	2.40	35.8	0.5
Tep2-29.1	0.06657	0.00136	174.05	2.91	36.0	0.6
Tep2-30.1	0.41864	0.04978	100.33	4.56	33.8	4.3
Tep2-31.1	0.07424	0.00190	172.13	2.34	36.0	0.5
Tep2-32.1	0.05425	0.00083	165.23	2.18	38.5	0.5
Tep2-33.1	0.06040	0.00189	176.20	2.79	35.8	0.6
Tep2-34.1	0.05339	0.00182	166.35	2.65	38.3	0.6
Tep2-35.1	0.10038	0.00512	166.84	2.96	35.9	0.7

[1]207 corrected.

TABLE A6. TEP3 Tera-Wasserburg Data

Sample	$^{207}Pb/^{206}Pb$	± 7/6	$^{238}U/^{206}Pb$	± 38/6	Age 38/6[1]	± age 38/6
Tep3-1.1	0.05397	0.00199	174.63	3.19	36.5	0.7
Tep3-2.1	0.32451	0.00380	101.88	1.77	40.9	0.8
Tep3-3.1	0.10458	0.00279	127.99	2.79	46.5	1.0
Tep3-3.2	0.07870	0.00435	149.91	17.81	41.1	4.9
Tep3-4.1	0.06101	0.00083	126.75	2.01	49.8	0.8
Tep3-5.1	0.04890	0.00069	151.08	3.56	42.4	1.0
Tep3-6.1	0.04984	0.00060	131.36	2.07	48.7	0.8
Tep3-7.1	0.04957	0.00068	151.82	1.73	42.2	0.5
Tep3-8.1	0.05425	0.00090	140.74	1.52	45.2	0.5
Tep3-9.1	0.05017	0.00112	156.59	2.68	40.9	0.7
Tep3-10.1	0.04861	0.00074	163.62	2.66	39.2	0.6
Tep3-11.1	0.05222	0.00093	145.97	2.02	43.7	0.6
Tep3-20.1	0.06029	0.00128	142.68	1.83	44.3	0.6
Tep3-21.1	0.06325	0.00300	25.52	20.21	244.1	192.6
Tep3-22.1	0.07504	0.00218	163.70	2.81	37.9	0.7
Tep3-23.1	0.05416	0.00128	152.26	2.30	41.8	0.6
Tep3-24.1	0.11056	0.00285	150.85	2.36	39.2	0.6
Tep3-25.1	0.09099	0.00594	154.59	2.17	39.2	0.6
Tep3-26.1	0.06110	0.00202	155.51	2.15	40.6	0.6
Tep3-27.1	0.05086	0.00071	142.55	1.71	44.8	0.5
Tep3-28.1	0.05262	0.00151	118.97	3.89	53.6	1.8
Tep3-29.1	0.08375	0.00492	156.70	3.10	39.1	0.8
Tep3-30.1	0.05099	0.00234	155.39	2.12	41.1	0.6
Tep3-31.1	0.05196	0.00191	150.22	2.19	42.5	0.6
Tep3-32.1	0.06760	0.00172	152.78	1.73	41.0	0.5
Tep3-33.1	0.05836	0.00102	153.59	2.43	41.2	0.6

[1]207 corrected.

TABLE A7. PCMG Wetherill Data

Sample	$^{206}Pb/^{238}U$	± 6/38	$^{207}Pb/^{235}U$	± 7/35	$^{207}Pb/^{206}Pb$	± 7/6
PCMG-1.1	0.42403	0.01647	10.0190	0.4159	0.17137	0.00181
PCMG-2.1	0.09048	0.00317	1.8476	0.0725	0.14810	0.00206
PCMG-3.1	0.04763	0.00174	0.8050	0.0451	0.12258	0.00468
PCMG-4.1	0.08353	0.00360	1.7435	0.0905	0.15139	0.00364
PCMG-5.1	0.02510	0.00121	0.3141	0.0588	0.09076	0.01587
PCMG-6.1	0.12727	0.00484	2.1443	0.1288	0.12220	0.00513
PCMG-7.1	0.15696	0.00553	2.8460	0.1172	0.13150	0.00228
PCMG-13.2	0.49926	0.02010	12.1800	0.5197	0.17693	0.00177
PCMG-18.1	0.10446	0.00374	2.2427	0.0902	0.15571	0.00223
PCMG-19.1	0.06973	0.00250	1.3327	0.0540	0.13862	0.00208
PCMG-20.1	0.11839	0.00427	2.4662	0.0952	0.15108	0.00152
PCMG-21.1	0.23074	0.00860	5.5392	0.2193	0.17411	0.00165
PCMG-22.1	0.12818	0.00454	2.8341	0.1076	0.16036	0.00159
PCMG-22.2	0.23664	0.00853	5.4402	0.2054	0.16674	0.00125
PCMG-23.1	0.09643	0.00405	1.9342	0.0919	0.14547	0.00255
PCMG-23.2	0.32280	0.01161	7.6032	0.2838	0.17083	0.00110
PCMG-24.1	0.20461	0.00724	4.5968	0.1750	0.16294	0.00167
PCMG-25.1	0.41329	0.01436	10.2460	0.3717	0.17980	0.00125
PCMG-26.1	0.10430	0.00378	2.2066	0.0929	0.15345	0.00266
PCMG-27.1	0.44841	0.01569	11.2450	0.4082	0.18188	0.00114
PCMG-28.1	0.49669	0.01841	12.4870	0.4887	0.18234	0.00159
PCMG-29.1	0.35543	0.01252	8.1954	0.2956	0.16723	0.00076
PCMG-30.1	0.52561	0.01865	13.3700	0.5122	0.18449	0.00197
PCMG-30.1	0.50752	0.01862	12.8120	0.5003	0.18309	0.00175

Age 6/38 ± age 6/38

TABLE A7. *Continued*

Age 6/38	± age 6/38	Age 7/35	± age 7/35	Age 7/6	± age 7/6
721.29	24.65	1262.2	28.3	2358.2	17.3
1338.40	45.21	1906.7	34.6	2597.5	15.9
777.48	26.00	1364.6	28.9	2459.4	16.8
1369.20	44.64	1891.2	32.9	2525.1	12.7
593.48	23.87	1093.0	32.3	2293.3	30.5
1803.40	56.83	2185.2	34.1	2565.8	10.8
1200.10	38.88	1748.7	32.3	2486.4	17.4
2229.90	65.83	2457.2	34.1	2651.0	11.6
639.53	22.12	1183.1	29.9	2384.7	29.8
2388.20	70.20	2543.7	34.4	2670.1	10.4
2599.60	79.79	2641.8	37.5	2674.3	14.6
1960.50	59.81	2252.8	33.2	2530.1	7.6
2722.90	79.28	2706.2	36.9	2693.7	17.7
2646.00	80.11	2665.9	37.5	2681.0	15.9